

Chapter 1

Quantum Metrology with Cold Atoms

Jiahao Huang, Shuyuan Wu, Honghua Zhong, and Chaohong Lee*
*State Key Laboratory of Optoelectronic Materials and Technologies,
 School of Physics and Engineering, Sun Yat-Sen University, Guangzhou
 510275, China
 chleecn@gmail.com*

Quantum metrology is the science that aims to achieve precision measurements by making use of quantum principles. Attribute to the well-developed techniques of manipulating and detecting cold atoms, cold atomic systems provide an excellent platform for implementing precision quantum metrology. In this chapter, we review the general procedures of quantum metrology and some experimental progresses in quantum metrology with cold atoms. Firstly, we give the general framework of quantum metrology and the calculation of quantum Fisher information, which is the core of quantum parameter estimation. Then, we introduce the quantum interferometry with single and multiparticle states. In particular, for some typical multiparticle states, we analyze their ultimate precision limits and show how quantum entanglement could enhance the measurement precision beyond the standard quantum limit. Further, we review some experimental progresses in quantum metrology with cold atomic systems.

Contents

1. Quantum Metrology with Cold Atoms	1
<i>J. Huang, S. Wu, H. Zhong, and C. Lee</i>	
1. Introduction	2
2. Quantum Metrology	3
2.1. Measurement in Quantum Mechanics	3
2.2. General Procedure of Measurements	4
2.3. Parameter Estimation	5
2.3.1. Parameter estimation in classical statistics	6

*Corresponding author.

2.3.2. Parameter estimation in quantum mechanics	9
3. Quantum Interferometry with Single-Particle States	12
3.1. Mach-Zehnder interferometry	12
3.2. Ramsey interferometry	14
4. Quantum Interferometry with Multiparticle States	16
4.1. Spin coherent states	17
4.2. Spin squeezed states	20
4.3. NOON states	23
4.4. Entangled coherent states	24
4.5. Twin Fock states	25
5. Experimental Progresses	27
5.1. Bose-Einstein condensed atoms	27
5.1.1. Nonlinear interferometry with spin squeezed states	28
5.1.2. Twin matter-wave interferometry	34
5.2. Ultracold trapped ions	35
5.3. Cold atomic ensembles	37
6. Summary and discussion	38
References	40

1. Introduction

In recent years, the experimental techniques of manipulating cold atoms have been dramatically developed. Therefore, beyond exploring their quantum nature, it becomes possible to engineer cold atoms¹⁻³ for practical technology applications.^{4,5} Naturally, because of their robust quantum coherence and high controllability, cold atoms could be engineered to achieve high precision metrology at the level of quantum mechanics.⁶⁻¹⁰

Quantum metrology¹¹⁻¹³ aims to yield high measurement precisions by taking advantage of the quantum principles. A central goal of quantum metrology is how to enhance measurement precision with quantum resources such as spin squeezing and multiparticle entanglement.¹¹⁻²⁶ For a multiparticle system of cold atoms, it has been demonstrated that quantum entanglement and spin squeezing can be prepared by employing intrinsic inter-atom interactions or laser induced artificial inter-atom interactions.²⁷⁻²⁹ Up to now, cold atoms have been widely used for implementing precision metrology, such as interferometers,³⁰⁻³² gyroscopes,³³ quantum clocks,³⁴⁻³⁶ magnetic field detectors³⁷⁻⁴⁰ and micro-gravity sensors.⁴¹⁻⁴⁴

In this chapter, we review the recent progresses in quantum metrology with cold atoms. In Sec. 2, we present the general framework of quantum metrology. In particular, we give the general procedure of measurement in quantum mechanics and the fundamental theory of parameter estimation. In Sec. 3, we describe the basic principles of quantum interferometry with single-particle states, which includes the Ramsey interferometry and Mach-

Zehnder interferometry. In Sec. 4, we show the basic principles of quantum interferometry with multiparticle states, such as, spin coherent states, spin squeezed states, NOON states, entangled coherent states and twin Fock states. In Sec. 5, we mention some key experimental progresses in quantum metrology with various cold atomic systems, such as, ultracold trapped ions, cold atomic ensembles and Bose-Einstein condensed atoms. In the last section, we briefly summarize this review and discuss some related problems.

2. Quantum Metrology

2.1. *Measurement in Quantum Mechanics*

At the level of physics, a measurement is a physical process which estimates the quantity of a particular observable (or a physical parameter).⁴⁵ It plays a key role in most natural sciences and practical technologies. To compare different measurements, one has to specify magnitude, units and uncertainty for a particular measurement. The science of measurement is called metrology.

The measurement process is governed by the laws of physics. Therefore, the measurement precision depends on both the performance imperfections and the fundamental limit imposed by the physical laws. The statistical fluctuations can be reduced by repeating the same measurement over times and averaging the results.^{13,46} According to the central limit theorem, for N repetitions of the same measurement, the statistical fluctuation scales as $1/\sqrt{N}$ which is called the shot noise limit (SNL).¹¹

In quantum mechanics, a measurement process is the action that determines a particular observable (or a physical parameter) of a quantum system. Quantum metrology aims to make high-precision measurements with quantum resources such as entanglement and squeezing. It has been demonstrated that quantum metrology could give better precision than the same measurement performed in a classical framework. For an example, the measurement precision of a Mach-Zehnder interferometer of N independent particles is limited by the standard quantum limit (SQL), which has the same scaling $1/\sqrt{N}$ as the SNL. However, the measurement precision of a Mach-Zehnder interferometer of N entangled particles in the NOON state can reach the Heisenberg limit which has scaling $1/N$.⁴⁷⁻⁴⁹ Similar precision enhancements can also be obtained by other non-classical states such as spin squeezed states.⁵⁰

2.2. General Procedure of Measurements

Usually, a general measurement process includes three steps.^{12,13,51,52} First, prepare the probe into a desired initial state. Second, let the probe undergo a dynamical evolution dependent on the physical parameter to be measured. Third, read out the final state of the probe and estimate the physical parameter with the extracted information.

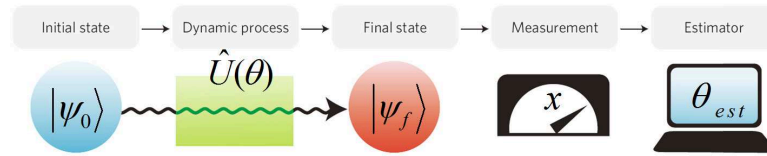


Fig. 1. The general procedure for a measurement process in quantum mechanics. An initial state is sent through a physical channel and evolves into the final state under a parameter-dependent dynamical process. Then, the final state is read out and the unknown parameter is estimated. From Ref. 52.

The density matrix of the initial state $|\psi_0\rangle$ for the probe can be expressed as,

$$\rho_0 = |\psi_0\rangle\langle\psi_0|. \quad (1)$$

The initial state is sent into a dynamical process dependent upon an unknown parameter θ to be measured. The initial state $|\psi_0\rangle$ evolves into the final state $|\psi(\theta)\rangle$ under the action of the parameter-dependent evolution operator $\hat{U}(\theta)$. If the evolution is unitary, the density matrix for the final state is given by,

$$\rho(\theta) = |\psi(\theta)\rangle\langle\psi(\theta)| = \hat{U}(\theta)\rho_0\hat{U}^\dagger(\theta). \quad (2)$$

Then, a measurement of a suitable observable \hat{O} is made on the final state $|\psi(\theta)\rangle$. To successfully extract the unknown parameter θ , the observable \hat{O} should have θ -dependent expectation values $\langle\hat{O}\rangle$.

If one has a prior knowledge of the evolution and the dependence of the observable expectation $\langle\hat{O}\rangle$ on the parameter θ , the information of the parameter θ can be revealed according to the measurement results of the observable \hat{O} . According to the error propagation formula, the standard deviation of the parameter is given by

$$\Delta\theta = \frac{\Delta\hat{O}}{\left|\frac{\partial\langle\hat{O}\rangle}{\partial\theta}\right|}, \quad (3)$$

where the standard deviation of the observable is defined as

$$\Delta\hat{O} = \sqrt{\langle\hat{O}^2\rangle - \langle\hat{O}\rangle^2} \quad (4)$$

with

$$\langle\hat{O}\rangle = \langle\psi(\theta)|\hat{O}|\psi(\theta)\rangle, \quad (5)$$

$$\langle\hat{O}^2\rangle = \langle\psi(\theta)|\hat{O}^2|\psi(\theta)\rangle. \quad (6)$$

It clearly shows that the standard deviation of the parameter $\Delta\theta$ is dependent on θ itself. In addition, the minimum standard deviation of the parameter $\Delta\theta$ corresponds to the maximum slope of the expectation value with respect to the parameter θ , $|\partial\langle\hat{O}\rangle/\partial\theta|$.

2.3. Parameter Estimation

Usually, measurement data are a set of random outputs from a particular effect dependent on the parameter to be estimated. The process of parameter estimation is using the information of a set of measurement data to estimate the value of the parameter. As several physical parameters can not be directly measured, one has to use indirect measurements, that is, inferring the parameter value from an estimator which is a function of the measurement data of a single observable or a set of observables.

There are two typical paradigms for implementing parameter estimation: global and local ones. In the global approach, an estimator which is independent on the value of the parameter is used to minimize a suitable cost function averaged all possible values of the parameter. In the local approach, an estimator which has minimum variance at a fixed value of the parameter is used to maximize the Fisher information. In most cases, since the optimization concerns a specific value of the parameter, the local approach is expected to provide a better ultimate bound on measurement precision. Below, we concentrate our discussion on the local approach.⁵²⁻⁵⁴

In a realistic estimation, one measures a suitable observable X at first and then estimates the unknown parameter θ by an estimator function $\theta_{est} = T(X)$. Therefore, the deviation of an estimation is given by,^{55,57}

$$\delta\theta \equiv \frac{\theta_{est}}{|d\langle\theta_{est}\rangle/d\theta|} - \theta, \quad (7)$$

where θ_{est} and θ are the estimated and the actual values of the parameter, respectively. In the case of unbiased estimators, $\langle\theta_{est}\rangle = \theta$, it is just the difference between the estimated and the actual values of the parameter.

2.3.1. Parameter estimation in classical statistics

We consider the problem of estimating a single parameter with a set of measurement data from v times of identical experiments (or one experiment of v independent and identical probes). The measurement precision $\Delta\theta$ of an unknown parameter θ is limited by the Cramér-Rao bound:^{55,58,59}

$$\Delta\theta = \sqrt{\langle(\delta\theta)^2\rangle} \geq \frac{1}{\sqrt{vF(\theta)}}. \quad (8)$$

Here, $F(\theta)$ is called the Fisher information, which is a measure of the ability to estimate a parameter θ .^{60,61} Obviously, the optimal measurement precision can be obtained by maximizing the Fisher information.

If the measured observable X has N different discrete values (x_1, x_2, \dots, x_N) , the Fisher information $F(\theta)$ is expressed as

$$F(\theta) \equiv \sum_{i=1}^N P(x_i|\theta) \left(\frac{\partial \ln[P(x_i|\theta)]}{\partial \theta} \right)^2 \quad (9)$$

with $P(x_i|\theta)$ denoting the conditional probability of the measurement data x_i given the parameter θ .

If the measured observable X is a continuous variable x , the Fisher information $F(\theta)$ reads as

$$F(\theta) \equiv \int dx p(x|\theta) \left(\frac{\partial \ln[p(x|\theta)]}{\partial \theta} \right)^2 \quad (10)$$

with $p(x|\theta)$ denoting the conditional probability density of the measurement data x given the parameter θ . Thus $p(x|\theta)dx$ represents the conditional probability of the measurement data between x and $x+dx$ given the parameter θ .

Now, we show why the Cramér-Rao bound gives the minimum uncertainty of the estimated parameter.^{54,55,59,62} We consider a set of measurement data (X_1, X_2, \dots, X_v) obtained from v identical experiments (or one experiment of v independent and identical probes). The parameter θ is estimated by a function constructed from the measurement data

$$\theta_{est} = T(x_1^{n_1}, x_2^{n_2}, \dots, x_v^{n_v}), \quad (11)$$

where $x_j^{n_j}$ is the n_j -th value of X_j with $j = (1, 2, \dots, v)$. Therefore, the averaged value of θ_{est} is given as

$$\langle \theta_{est} \rangle = \sum_{n_1, n_2, \dots, n_v} T(x_1^{n_1}, x_2^{n_2}, \dots, x_v^{n_v}) P(x_1^{n_1}|\theta) P(x_2^{n_2}|\theta) \dots P(x_v^{n_v}|\theta). \quad (12)$$

Obviously, the estimation function θ_{est} does not depend on the parameter θ , but the average $\langle \theta_{est} \rangle$ depends on the parameter θ .

Defining the deviation, $\delta\theta_{est} = \theta_{est} - \langle \theta_{est} \rangle$, one can easily find

$$\sum_{n_1, n_2, \dots, n_v} P(x_1^{n_1} | \theta) P(x_2^{n_2} | \theta) \cdots P(x_v^{n_v} | \theta) \delta\theta_{est} = 0. \quad (13)$$

According to the chain rule and $\partial\theta_{est}/\partial\theta = 0$, its derivative with respect to the parameter θ reads as,

$$\begin{aligned} \sum_{n_1, n_2, \dots, n_v} \{ & P(x_1^{n_1} | \theta) P(x_2^{n_2} | \theta) \cdots P(x_v^{n_v} | \theta) \\ & \times \left[\sum_{i=1}^v \frac{1}{P(x_i^{n_i} | \theta)} \frac{\partial P(x_i^{n_i} | \theta)}{\partial \theta} \right] \delta\theta_{est} \} - \frac{d\langle \theta_{est} \rangle}{d\theta} = 0. \end{aligned} \quad (14)$$

Therefore,

$$\begin{aligned} \frac{d\langle \theta_{est} \rangle}{d\theta} = \sum_{n_1, n_2, \dots, n_v} \{ & P(x_1^{n_1} | \theta) P(x_2^{n_2} | \theta) \cdots P(x_v^{n_v} | \theta) \\ & \times \left(\sum_{i=1}^v \frac{\partial \ln [P(x_i^{n_i} | \theta)]}{\partial \theta} \right) \delta\theta_{est} \}. \end{aligned} \quad (15)$$

By applying the inequality $\langle AB \rangle^2 \leq \langle A^2 \rangle \langle B^2 \rangle$ to the right-hand side of the above equation, one can obtain

$$\begin{aligned} \left\{ \sum_{n_1, n_2, \dots, n_v} P(x_1^{n_1} | \theta) P(x_2^{n_2} | \theta) \cdots P(x_v^{n_v} | \theta) \left(\sum_{i=1}^v \frac{\partial \ln [P(x_i^{n_i} | \theta)]}{\partial \theta} \right)^2 \right\} \times \\ \left\{ \sum_{n_1, n_2, \dots, n_v} P(x_1^{n_1} | \theta) P(x_2^{n_2} | \theta) \cdots P(x_v^{n_v} | \theta) (\delta\theta_{est})^2 \right\} \geq \left(\frac{d\langle \theta_{est} \rangle}{d\theta} \right)^2 \end{aligned} \quad (16)$$

Since

$$\sum_{n_i} P(x_i^{n_i} | \theta) \frac{\partial \ln [P(x_i^{n_i} | \theta)]}{\partial \theta} = \sum_{n_i} \frac{\partial P(x_i^{n_i} | \theta)}{\partial \theta} = \frac{d}{d\theta} \sum_{n_i} P(x_i^{n_i} | \theta) = 0, \quad (17)$$

all cross terms in the right-hand side of Eq. (16) vanish, and the square of the sum reduces to

$$\begin{aligned} \left\{ \sum_{n_1, n_2, \dots, n_v} P(x_1^{n_1} | \theta) P(x_2^{n_2} | \theta) \cdots P(x_v^{n_v} | \theta) \sum_{i=1}^v \left(\frac{\partial \ln [P(x_i^{n_i} | \theta)]}{\partial \theta} \right)^2 \right\} \times \\ \left\{ \sum_{n_1, n_2, \dots, n_v} P(x_1^{n_1} | \theta) P(x_2^{n_2} | \theta) \cdots P(x_v^{n_v} | \theta) (\delta\theta_{est})^2 \right\} \geq \left(\frac{d\langle \theta_{est} \rangle}{d\theta} \right)^2 \end{aligned} \quad (18)$$

Denoting the averaged square deviation of θ_{est} as

$$\langle (\delta\theta_{est})^2 \rangle = \sum_{n_1, n_2, \dots, n_v} P(x_1^{n_1} | \theta) P(x_2^{n_2} | \theta) \cdots P(x_v^{n_v} | \theta) (\delta\theta_{est})^2, \quad (19)$$

one can obtain

$$\left\{ \sum_{n_1, n_2, \dots, n_v} P(x_1^{n_1} | \theta) P(x_2^{n_2} | \theta) \cdots P(x_v^{n_v} | \theta) \sum_{i=1}^v \left(\frac{\partial \ln [P(x_i^{n_i} | \theta)]}{\partial \theta} \right)^2 \right\} \times \langle (\delta\theta_{est})^2 \rangle \geq \left(\frac{d \langle \theta_{est} \rangle}{d\theta} \right)^2. \quad (20)$$

As the measurement data (X_1, X_2, \dots, X_v) are independent and the sum for each X_j has the same form of the Fisher information (9), the above inequality becomes

$$vF(\theta) \langle (\delta\theta_{est})^2 \rangle \geq \left(\frac{d \langle \theta_{est} \rangle}{d\theta} \right)^2. \quad (21)$$

It can also be written in the form of

$$\frac{\langle (\delta\theta_{est})^2 \rangle}{(d \langle \theta_{est} \rangle / d\theta)^2} \geq \frac{1}{vF(\theta)}. \quad (22)$$

To show how the estimated parameter is close to the actual one, the uncertainty given in Eq. (7) should be calculated. The average of the square of Eq. (7) is given as

$$\langle (\delta\theta)^2 \rangle = \frac{\langle \delta\theta_{est}^2 \rangle}{(d \langle \theta_{est} \rangle / d\theta)^2} + \langle \delta\theta \rangle^2. \quad (23)$$

Substituting Eq. (23) into Eq. (22), the inequality reads as

$$\langle (\delta\theta)^2 \rangle \geq \frac{1}{vF(\theta)} + \langle \delta\theta \rangle^2. \quad (24)$$

In general, we regard the expectation of the unknown estimated parameter over many times as the actual one, i.e., $\langle \theta_{est} \rangle = \theta$. Therefore, the derivative $d \langle \theta_{est} \rangle / d\theta = 1$, $\langle \delta\theta \rangle^2 = 0$, and $\langle (\delta\theta)^2 \rangle$ reduces to the variance $(\Delta\theta)^2$. That is, the above inequality becomes

$$(\Delta\theta)^2 = \langle (\delta\theta)^2 \rangle \geq \frac{1}{vF(\theta)}, \quad (25)$$

whose square root,

$$\Delta\theta = \sqrt{\langle (\delta\theta)^2 \rangle} \geq \frac{1}{\sqrt{vF(\theta)}}, \quad (26)$$

gives the so-called Cramér-Rao bound.

If the measured observable X is a continuous variable x , the deviation of the Cramér-Rao bound can be obtained by replacing the sum $\sum_{n_1, n_2, \dots, n_v}$ with the integral $\int dx_1 dx_2 \cdots dx_v$. The form of the Cramér-Rao bound is as same as the formula (26) and the corresponding Fisher information is given by the formula (10).

2.3.2. Parameter estimation in quantum mechanics

In quantum mechanics, a generalized measurement can be described by a set of Hermitian operators $\hat{E}(X)$, which are Positive-Operator Valued Measures (POVM).⁶³ Here, X is the measured observable. If X has N different discrete values (x_1, x_2, \dots, x_N) , the operators $\hat{E}(x_n)$ satisfy,

$$\hat{E}(x_n) \geq 0, \quad \sum_{n=1}^N \hat{E}(x_n) = \mathbf{1}, \quad (27)$$

where $\mathbf{1}$ is the identity operator. If X has continuous values x , the operators $\hat{E}(x)$ satisfy,

$$\hat{E}(x) \geq 0, \quad \int dx \hat{E}(x) = \mathbf{1}. \quad (28)$$

The above relations ensure non-negative probabilities and unitary total probability.

The probability of getting a particular measurement data x_n on a state $|\psi\rangle$ is given by,

$$P(x_n) = \langle \psi | \hat{E}(x_n) | \psi \rangle = \text{Tr}[\rho \hat{E}(x_n)], \quad (29)$$

where $\rho = |\psi\rangle\langle\psi|$ is the density matrix. Therefore, by making a measurement on the final state, one can obtain the conditional probability of the measurement data x_n given the parameter θ ,

$$P(x_n|\theta) = \langle \psi(\theta) | \hat{E}(x_n) | \psi(\theta) \rangle = \text{Tr}[\rho(\theta) \hat{E}(x_n)]. \quad (30)$$

If X has continuous values x , the corresponding conditional probability density of the measurement data x given the parameter θ reads as,

$$p(x|\theta) = \langle \psi(\theta) | \hat{E}(x) | \psi(\theta) \rangle = \text{Tr}[\rho(\theta) \hat{E}(x)]. \quad (31)$$

According to the definition of the Fisher information (9), one can find that $F(\theta)$ is a function of all conditional probabilities $P(x_n|\theta)$ which depend on the final state $|\psi(\theta)\rangle$ and the POVM $\hat{E}(x_n)$. Therefore, to optimize the Fisher information, we need to construct a suitable state and

measure a suitable observable. Further, for a given final state, the Fisher information can be maximized by trying different measurement strategies. The maximum of the Fisher information through out all possible quantum measurement strategies is called the quantum Fisher information,^{53,55,56}

$$F_Q(\theta) \equiv \max_{\{\hat{E}(x_n)\}} F[\theta; \{\hat{E}(x_n)\}], \quad (32)$$

where $\{\hat{E}(x_n)\} = (\hat{E}(x_1), \hat{E}(x_2), \dots, \hat{E}(x_N))$. The corresponding Cramér-Rao bound is called the quantum Cramér-Rao bound,

$$\Delta\theta = \sqrt{\langle(\delta\theta)^2\rangle} \geq \frac{1}{\sqrt{vF_Q(\theta)}}. \quad (33)$$

We now show how to derive the quantum Fisher information and the quantum Cramér-Rao bound for a pure state under a unitary evolution.⁶² Here, we consider a probe in the initial state $|\psi_0\rangle$ undergoing an evolution described by the operator $\hat{U}(\theta) = \exp(-i\hat{H}\theta)$ with the generator \hat{H} . Inserting the density matrix (2) into the conditional probability (30), we obtain

$$\begin{aligned} \frac{\partial P(x_n|\theta)}{\partial\theta} &= \left[\frac{d}{d\theta} \langle\psi(\theta)| \right] \hat{E}(x_n) |\psi(\theta)\rangle + \langle\psi(\theta)| \hat{E}(x_n) \left[\frac{d}{d\theta} |\psi(\theta)\rangle \right] \\ &= i\langle\psi(\theta)| \hat{H} \hat{E}(x_n) |\psi(\theta)\rangle - i\langle\psi(\theta)| \hat{E}(x_n) \hat{H} |\psi(\theta)\rangle \\ &= i\langle\psi(\theta)| [\hat{H}, \hat{E}(x_n)] |\psi(\theta)\rangle \\ &= -2\text{Im} [\langle\psi(\theta)| \hat{H} \hat{E}(x_n) |\psi(\theta)\rangle]. \end{aligned} \quad (34)$$

Introducing an arbitrary real function $G(\theta)$ into Eq. (34), we have

$$\frac{\partial P(x_n|\theta)}{\partial\theta} = -2\text{Im} \left\{ \langle\psi(\theta)| [\hat{H} - G(\theta)] \hat{E}(x_n) |\psi(\theta)\rangle \right\}, \quad (35)$$

and so that

$$\begin{aligned} \left(\frac{\partial P(x_n|\theta)}{\partial\theta} \right)^2 &= 4 \left\{ \text{Im} \left\{ \langle\psi(\theta)| [\hat{H} - G(\theta)] \hat{E}(x_n) |\psi(\theta)\rangle \right\} \right\}^2 \\ &\leq 4 |\langle\psi(\theta)| [\hat{H} - G(\theta)] \hat{E}(x_n) |\psi(\theta)\rangle|^2 \\ &\leq 4 \langle\psi(\theta)| \hat{E}(x_n) |\psi(\theta)\rangle \langle\psi(\theta)| [\hat{H} - G(\theta)] \hat{E}(x_n) [\hat{H} - G(\theta)] |\psi(\theta)\rangle \\ &= 4P(x_n|\theta) \langle\psi(\theta)| [\hat{H} - G(\theta)] \hat{E}(x_n) [\hat{H} - G(\theta)] |\psi(\theta)\rangle. \end{aligned} \quad (36)$$

Therefore, one can obtain

$$\begin{aligned}
 F(\theta) &= \sum_n \frac{1}{P(x_n|\theta)} \left[\frac{\partial P(x_n|\theta)}{\partial \theta} \right]^2 \\
 &\leq 4 \sum_n \langle \psi(\theta) | [\hat{H} - G(\theta)] \hat{E}(x_n) [\hat{H} - G(\theta)] | \psi(\theta) \rangle \\
 &= 4 \langle \psi(\theta) | [\hat{H} - G(\theta)]^2 | \psi(\theta) \rangle.
 \end{aligned} \tag{37}$$

If X has continuous values, the corresponding Fisher information reads as

$$\begin{aligned}
 F(\theta) &= \int dx \frac{1}{p(x|\theta)} \left[\frac{\partial p(x|\theta)}{\partial \theta} \right]^2 \\
 &\leq 4 \int dx \langle \psi(\theta) | [\hat{H} - G(\theta)] \hat{E}(x) [\hat{H} - G(\theta)] | \psi(\theta) \rangle \\
 &= 4 \langle \psi(\theta) | [\hat{H} - G(\theta)]^2 | \psi(\theta) \rangle.
 \end{aligned} \tag{38}$$

If we choose $G(\theta) = \langle \psi_0 | \hat{H} | \psi_0 \rangle$, due to $\langle \hat{H} \rangle = \langle \psi_0 | \hat{H} | \psi_0 \rangle = \langle \psi(\theta) | \hat{H} | \psi(\theta) \rangle$, the Fisher information attains its minimum and the above inequality reads as

$$F(\theta) \leq 4 \langle \psi_0 | (\Delta \hat{H})^2 | \psi_0 \rangle \tag{39}$$

with $\Delta \hat{H} = \hat{H} - \langle \hat{H} \rangle$. Therefore, the quantum Fisher information for a pure state can be defined as

$$F_Q(\theta) = 4 \langle \psi_0 | (\Delta \hat{H})^2 | \psi_0 \rangle, \tag{40}$$

which is a function of the generator \hat{H} and the initial state $|\psi_0\rangle$.

By using $|\psi(\theta)\rangle = \hat{U} |\psi_0\rangle = \exp(-i\hat{H}\theta) |\psi_0\rangle$ and $|\psi'(\theta)\rangle = \frac{d}{d\theta} |\psi(\theta)\rangle = (-i\hat{H}) |\psi(\theta)\rangle$, the quantum Fisher information can be expressed as

$$F_Q(\theta) = 4 \left[\langle \psi'(\theta) | \psi'(\theta) \rangle - |\langle \psi'(\theta) | \psi(\theta) \rangle|^2 \right], \tag{41}$$

which is a function of the final state $|\psi(\theta)\rangle$ and its derivative with respect to the parameter θ .

The quantum Fisher information provides a powerful tool for parameter estimation only dependent on the state of the system but not on the procedure of measurement.⁶⁷⁻⁷⁰ As long as the initial state and the final state of the probe after the parameter-dependent evolution are known, one can immediately predict the minimum uncertainty of the parameter to be estimated. Generally speaking, the quantum Cramér-Rao bound is the ultimate bound on the parameter uncertainty, and the parameter uncertainty in realistic measurements may be larger.

3. Quantum Interferometry with Single-Particle States

Interferometry is an important and most used method for implementing measurements.^{71–74} Interferometry via quantum states includes three key steps: (i) splitting the initial state into two modes, (ii) undergoing a period of free evolution and (iii) recombining two modes for readout. There are two typical types of interferometry. One is the Mach-Zehnder interferometry, which has extensive applications in phase shift measurements.^{75,76} The other is the Ramsey interferometry, which has been widely used in atomic-molecular experiments for precision spectroscopy and measurement.^{77–79} In this section, we briefly introduce these two kinds of interferometry with single-particle states.

It is well known that a two-mode (or two-level) quantum particle can be regarded as a spin- $\frac{1}{2}$ particle, which can be described by the three Pauli matrices $\hat{\sigma}_x$, $\hat{\sigma}_y$ and $\hat{\sigma}_z$.^{80,81} The two eigenstates $|\uparrow\rangle$ and $|\downarrow\rangle$ obey $\frac{\sigma_z}{2}|\uparrow\rangle = +\frac{1}{2}|\uparrow\rangle$ and $\frac{\sigma_z}{2}|\downarrow\rangle = -\frac{1}{2}|\downarrow\rangle$ and an arbitrary pure state can be written as $|\theta, \varphi\rangle = e^{i\gamma}(\sin\frac{\theta}{2}|\uparrow\rangle + \cos\frac{\theta}{2}e^{i\varphi}|\downarrow\rangle)$ with the common phase γ . The factor $e^{i\gamma}$ has no observable effects, thus the pure states $|\theta, \varphi\rangle$ with different values of γ are represented by the same classical spin $(S_x, S_y, S_z) = \frac{1}{2}(\sin\theta\cos\varphi, \sin\theta\sin\varphi, \cos\theta)$ in the Bloch sphere. Where, the longitudinal component $S_z = \cos\theta = \frac{1}{2}(\cos^2\frac{\theta}{2} - \sin^2\frac{\theta}{2})$ stands for the half population difference between the two eigenstates, and the transverse components (S_x, S_y) stand for the quantum coherence between the two modes. This means that the polar angle θ reflects the polarization information, while the azimuthal angle φ corresponds to coherence.

3.1. Mach-Zehnder interferometry

A conventional Mach-Zehnder interferometer is composed of two beam splitters and two propagation paths.^{75,83,84} A collimated beam of single particles is divided into two parts by a 50:50 beam splitter. Then the two parts pass through two different spatial paths and accumulate a relative phase shift between the two parts. At last, the two parts are recombined for interference via another 50:50 beam splitter. The phase difference can be extracted from the interference fringe.⁸⁵ The schematic diagram is shown in Fig. 2.

Suppose an atom incidents in the input port a , that is, the initial state of the atom is prepared in mode $|a\rangle$. The first beam splitter transforms the input state into an equal superposition state of the two involved modes $|a\rangle$

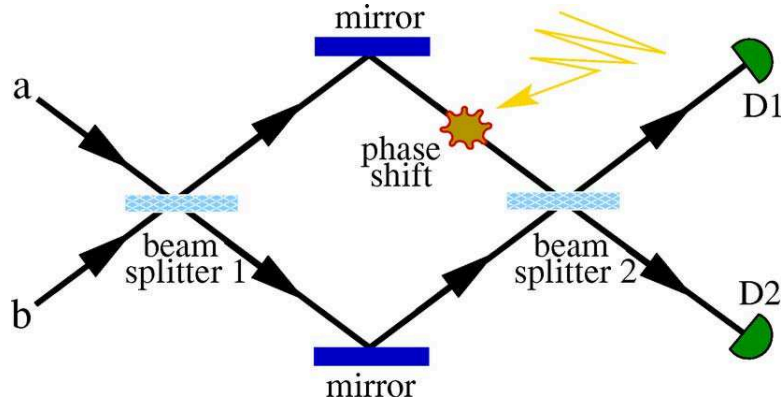


Fig. 2. Schematic diagram of a Mach-Zehnder interferometer. Single atoms/photons enter the input ports, combine in the first beam splitter, evolve in the two paths, recombine via the second beam splitter and are finally detected in $D1$ and $D2$. The phase shift is inferred from the number of atoms or photons measured in each output port. From Ref. 86.

and $|b\rangle$,

$$|\psi_{in}\rangle = \hat{T}|a\rangle = \frac{1}{\sqrt{2}}(|a\rangle + |b\rangle), \quad (42)$$

with the transformation matrix,

$$\hat{T} = \frac{1}{\sqrt{2}} \begin{pmatrix} 1 & 1 \\ 1 & -1 \end{pmatrix}. \quad (43)$$

Then the two modes propagate along different paths and accumulate a relative phase shift φ . That is, before entering into the second beam splitter, the state reads as

$$|\psi_{out}\rangle = \frac{1}{\sqrt{2}}(|a\rangle + e^{i\varphi}|b\rangle). \quad (44)$$

The second beam splitter recombines the two paths and the state is transformed into,

$$|\psi_f\rangle = \hat{T}\psi_{out} = \frac{1}{\sqrt{2}}[(1 + e^{i\varphi})|a\rangle + (1 - e^{i\varphi})|b\rangle]. \quad (45)$$

At last, the output state is detected by $D1$ and $D2$, which give $p(a|\varphi) = \cos^2(\varphi/2)$ for the probability of the atom in $|a\rangle$ and $p(b|\varphi) = \sin^2(\varphi/2)$ for the probability of the atom in $|b\rangle$.

From Eq. (10), the Fisher information for the above single-atom Mach-Zehnder interferometry can be obtained,

$$F(\varphi) = \frac{1}{p(a|\varphi)} \left[\frac{\partial p(a|\varphi)}{\partial \varphi} \right]^2 + \frac{1}{p(b|\varphi)} \left[\frac{\partial p(b|\varphi)}{\partial \varphi} \right]^2, \quad (46)$$

$$= \sin^2 \varphi + \cos^2 \varphi = 1.$$

Therefore, the minimal uncertainty of the relative phase is given as,

$$\delta\varphi = \frac{1}{\sqrt{F(\varphi)}} = 1. \quad (47)$$

Repeating the experiment N times, the uncertainty of the relative phase reads as,

$$\delta\varphi = \frac{1}{\sqrt{NF(\varphi)}} = \frac{1}{\sqrt{N}}, \quad (48)$$

which attains the so-called standard quantum limit (SQL).

3.2. Ramsey interferometry

The conventional Ramsey interferometry consists of two $\frac{\pi}{2}$ pulses and a free evolution process. In comparison with Mach-Zehnder interferometry, the two $\frac{\pi}{2}$ pulses act as the two beam splitters and the free evolution accumulate the relative phase between the two involved levels.⁸⁷⁻⁹⁰

We consider a two-level atom, which is initially prepared in its ground state $|\downarrow\rangle$. Without loss of generality, we assume that the eigen-energies for the ground state $|\downarrow\rangle$ and the excited state $|\uparrow\rangle$ are $-\frac{\omega_0}{2}$ and $+\frac{\omega_0}{2}$, respectively. The first $\frac{\pi}{2}$ pulse is applied and the state becomes

$$|\psi_{in}\rangle = \frac{1}{\sqrt{2}} (|\downarrow\rangle + |\uparrow\rangle), \quad (49)$$

which is an equal-probability superposition of the ground state $|\downarrow\rangle$ and the excited state $|\uparrow\rangle$. Then, the system undergoes a free evolution. In which, the ground state $|\downarrow\rangle$ accumulates a negative phase $-\frac{\varphi}{2}$, while the excited state $|\uparrow\rangle$ accumulates a positive phase $+\frac{\varphi}{2}$. Therefore, the state after the free evolution reads as,

$$|\psi_{out}\rangle = \frac{1}{\sqrt{2}} (e^{-i\varphi/2} |\downarrow\rangle + e^{+i\varphi/2} |\uparrow\rangle). \quad (50)$$

At last, the second $\frac{\pi}{2}$ pulse is applied and the final state is measured. The probability of the atom in the ground state $|\downarrow\rangle$ reads as,

$$p(\downarrow|\varphi) = \frac{1 + \cos \varphi}{2} = \cos^2 \frac{\varphi}{2}, \quad (51)$$

and the probability of the atom in the excited state $|\uparrow\rangle$ reads as,

$$p(\uparrow|\varphi) = 1 - p(\downarrow|\varphi) = \frac{1 - \cos\varphi}{2} = \sin^2\frac{\varphi}{2}. \quad (52)$$

The relative phase φ can be estimated from the probability $p(\downarrow|\varphi)$ or $p(\uparrow|\varphi)$. From Eq. (10), one can obtain the Fisher information for the above single-atom Ramsey interferometry,

$$\begin{aligned} F(\varphi) &= \frac{1}{p(\downarrow|\varphi)} \left[\frac{\partial p(\downarrow|\varphi)}{\partial\varphi} \right]^2 + \frac{1}{p(\uparrow|\varphi)} \left[\frac{\partial p(\uparrow|\varphi)}{\partial\varphi} \right]^2, \\ &= \sin^2\varphi + \cos^2\varphi = 1. \end{aligned} \quad (53)$$

Therefore, the minimal uncertainty of the relative phase is given by,

$$\delta\varphi = \frac{1}{\sqrt{F(\varphi)}} = 1. \quad (54)$$

Repeating the experiment N times, the uncertainty of the relative phase is limited by the standard quantum limit,

$$\delta\varphi = \frac{1}{\sqrt{NF(\varphi)}} = \frac{1}{\sqrt{N}}. \quad (55)$$

In the Bloch sphere, the initial state $|\downarrow\rangle$ is denoted by a spin vector pointing from the origin to the south pole. The first $\frac{\pi}{2}$ pulse rotates the state an angle $\frac{\pi}{2}$ around the y -axis. The free evolution rotates the state an angle φ around the z -axis. The second $\frac{\pi}{2}$ pulse rotates the state an angle $\frac{\pi}{2}$ around the y -axis. Lastly, the angle between the spin vector for the final state and the negative z -axis is just the angle φ .

The state evolution from the initial state to the final state can be described by,

$$|\psi_f\rangle = \hat{U}|\psi_0\rangle, \quad (56)$$

with the propagation operator

$$\hat{U} = \exp(-i\frac{\pi}{2}\hat{S}_y) \exp(-i\varphi\hat{S}_z) \exp(-i\frac{\pi}{2}\hat{S}_y). \quad (57)$$

Here, the spin operators are defined as $\hat{S}_{x,y,z} = \frac{1}{2}\hat{\sigma}_{x,y,z}$. Thus the expectation value for the final state reads as,

$$\langle\hat{S}_z\rangle_f = \langle\psi_f|\hat{S}_z|\psi_f\rangle = \langle\psi_0|\hat{U}^\dagger\hat{S}_z\hat{U}|\psi_0\rangle. \quad (58)$$

Substituting Eq. (57) into Eq. (58), we have

$$\langle\hat{S}_z\rangle_f = -\cos\varphi\langle\hat{S}_z\rangle_0 + \sin\varphi\langle\hat{S}_y\rangle_0 \quad (59)$$

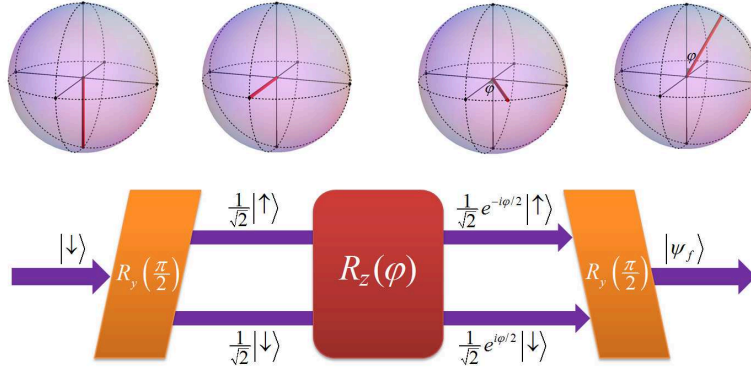


Fig. 3. Schematic diagram for a single-atom Ramsey interferometer. The two $\frac{\pi}{2}$ pulses and the free evolution are specific rotations in the geometrical representation via the Bloch sphere.

and

$$\begin{aligned} \left(\Delta\hat{S}_z\right)_f^2 &= \left(\Delta\hat{S}_z\right)_0^2 \cos^2 \varphi + \left(\Delta\hat{S}_y\right)_0^2 \sin^2 \varphi \\ &\quad - \sin \varphi \cos \varphi \left\langle \hat{S}_z \hat{S}_y + \hat{S}_y \hat{S}_z \right\rangle \end{aligned} \quad (60)$$

As the initial state $|\psi_0\rangle = |\downarrow\rangle_0$, we have

$$\langle \hat{S}_z \rangle_0 = \frac{1}{2}, \langle \hat{S}_z^2 \rangle_0 = \langle \hat{S}_y^2 \rangle_0 = \langle \hat{S}_x^2 \rangle_0 = \frac{1}{4}, \langle \hat{S}_x \rangle_0 = \langle \hat{S}_y \rangle_0 = 0.$$

Thus one can immediately obtain

$$\left(\Delta\hat{S}_z\right)_f = \frac{1}{2} \sin \varphi \quad (61)$$

According to Eq. (3), the standard deviation of φ is given by,

$$\Delta\varphi = \frac{\left(\Delta\hat{S}_z\right)_f}{\left|\partial\langle\hat{S}_z\rangle_f/\partial\varphi\right|} = 1, \quad (62)$$

which agrees with the minimal uncertainty given by the Fisher information Eq. (54). Repeating the measurement N times, the uncertainty can reach the standard quantum limit $\Delta\varphi \sim \frac{1}{\sqrt{N}}$.

4. Quantum Interferometry with Multiparticle States

In this section, we discuss the quantum interferometry with multiparticle states. There are many different types of multiparticle states that have been

used to implement quantum interferometry.^{91–106} Here, we concentrate our discussions on spin coherent states, spin squeezed states, NOON states, entangled coherent states and twin Fock states.

4.1. Spin coherent states

For an ensemble of N two-level particles, which can be regraded as N identical spin- $\frac{1}{2}$ particles, one can mathematically describe the system by a collective spin of length $J = \frac{N}{2}$.^{26,107} Such a spin- J system is characterized by three collective spin operators \hat{J}_x , \hat{J}_y and \hat{J}_z which are defined as the sum of spin operators of spin- $\frac{1}{2}$ spin operators \hat{S}_x , \hat{S}_y and \hat{S}_z ,

$$\hat{J}_i = \sum_{l=1}^N \hat{S}_i^{(l)}, (i = x, y, z). \quad (63)$$

By using the Schwinger representation,¹⁰⁸ the collective spin operators can be written in form of

$$\hat{J}_x = \frac{1}{2} (\hat{a}^\dagger \hat{b} + \hat{b}^\dagger \hat{a}), \quad (64)$$

$$\hat{J}_y = \frac{i}{2} (\hat{a}^\dagger \hat{b} - \hat{b}^\dagger \hat{a}) \quad (65)$$

$$\hat{J}_z = \frac{1}{2} (\hat{b}^\dagger \hat{b} - \hat{a}^\dagger \hat{a}) \quad (66)$$

in which the bosonic operators \hat{a}^\dagger (\hat{b}^\dagger) and \hat{a} (\hat{b}) denote the creation and annihilation operators for particles in $|\downarrow\rangle$ ($|\uparrow\rangle$), respectively.

The three collective spin operators obey the commutation relation,

$$[\hat{J}_\alpha, \hat{J}_\beta] = i\hbar \epsilon_{\alpha\beta\gamma} \hat{J}_\gamma (\alpha, \beta, \gamma = x, y, z) \quad (67)$$

where ϵ_{ijk} is the Levi-Civita symbol. Below, without loss of generality, we use the unit of $\hbar = 1$. Thus, the collective spin operators obey the uncertainty relation,

$$\Delta \hat{A} \Delta \hat{B} \geq \frac{1}{2} |\langle [\hat{A}, \hat{B}] \rangle|, \quad (68)$$

where $\Delta \hat{A}$ and $\Delta \hat{B}$ are standard deviations. Inserting Eq. (67) into Eq. (68), one can obtain the uncertainty relation

$$\Delta \hat{J}_\alpha \Delta \hat{J}_\beta \geq \frac{1}{2} |\langle \hat{J}_\gamma \rangle|, \quad (69)$$

for the three collective spin operators.

Coherent spin states (CSS) are the most ‘classical like’ pure quantum states of N spin- $\frac{1}{2}$ particles that polarize in the same single-particle state.¹⁰⁹ Therefore, an arbitrary CSS can be expressed as

$$|\theta, \varphi\rangle_{CSS} = \otimes_{l=1}^N \left[\sin(\theta/2)e^{-i\varphi} |\uparrow\rangle_l + \cos(\theta/2)e^{i\varphi/2} |\downarrow\rangle_l \right], \quad (70)$$

which can be generated from the all-spin-down state $|0, 0\rangle_{CSS} = \otimes_{l=1}^N |\downarrow\rangle_l$ by a unitary rotation with angles θ and φ . The direction from the origin to the point (θ, φ) on the Bloch sphere corresponds to the direction of the mean total spin $\langle J \rangle$, which is called the mean spin direction (MSD).

One can also express a CSS in terms of the Dicke basis $|J, m\rangle$. The Dicke states are defined by the common eigenstates of \hat{J}^2 and \hat{J}_z : $\hat{J}^2|J, m\rangle = J(J+1)|J, m\rangle$ and $\hat{J}_z|J, m\rangle = m|J, m\rangle$. Here, we have $J = N/2$ and $-N/2 \leq m \leq N/2$ with the total particle number N .¹⁰⁷ A general form of CSS in the Dicke basis reads as^{97,110}

$$|\theta, \varphi\rangle_{CSS} = \sum_{m=-J}^J C_m(\theta) e^{-i(J+m)\varphi} |J, m\rangle, \quad (71)$$

with the coefficients

$$\begin{aligned} C_m(\theta) &= \binom{2J}{J+m}^{\frac{1}{2}} \cos^{J-m}(\theta/2) \sin^{J+m}(\theta/2) \\ &= \left[\frac{(2J)!}{(J+m)!(J-m)!} \right]^{\frac{1}{2}} \cos^{J-m}(\theta/2) \sin^{J+m}(\theta/2), \end{aligned} \quad (72)$$

which is a binomial distribution.

One important feature of CSS is that all particles are independent and have no quantum correlations. Therefore, a CSS has equal variance $(\Delta \hat{J}_\perp)^2$ in any direction J_\perp orthogonal to the MSD (θ, φ) . The variance $(\Delta \hat{J}_\perp)^2$ is given by the sum of N variances $(\Delta \hat{S}_\perp)^2$ of individual spin- $\frac{1}{2}$ particles, that is,

$$(\Delta \hat{J}_\perp)^2 = N \times (\Delta \hat{S}_\perp)^2 = \frac{N}{4}. \quad (73)$$

Choosing the MSD along the z -axis, and the two orthogonal directions to the MSD along the x -axis and y -axis, we have

$$(\Delta \hat{J}_x)^2 = (\Delta \hat{J}_y)^2 = \frac{|\langle J_z \rangle|}{2} = \frac{N}{4}, \quad (74)$$

and

$$\Delta \hat{J}_x \Delta \hat{J}_y = \frac{|\langle J_z \rangle|}{2}. \quad (75)$$

This indicates that the CSS satisfies the minimal condition of the Heisenberg uncertainty relation, i.e., Eq. (67) takes the equal sign.

Similar to the state for a single spin- $\frac{1}{2}$ particle, $|\theta, \varphi\rangle_{CSS}$ can also be represented on a generalized Bloch sphere with a radius of the total spin length $J = N/2$. Given the polar angle θ and the azimuthal angle φ for a CSS, we have $\langle \hat{J}_x \rangle = J \cos \varphi \sin \theta$ and $\langle \hat{J}_y \rangle = J \sin \varphi \sin \theta$ and $\langle \hat{J}_z \rangle = J \cos \theta$.

The CSS can be used to perform the Ramsey interferometry.¹¹¹ The procedure of the Ramsey interferometry with a CSS is similar to the case of a single-particle state. Usually, the interferometry experiment starts from an initial state of all N atoms in the same internal state $|\downarrow\rangle$, that is, $|\Psi_0\rangle = \otimes_{i=1}^N |\downarrow\rangle_i$. Applying a $\frac{\pi}{2}$ pulse to couple the two involved internal states, one can obtain the CSS,

$$|\Psi_{in}\rangle = \otimes_{i=1}^N \left[\frac{1}{\sqrt{2}} (|\uparrow\rangle_i + |\downarrow\rangle_i) \right] \quad (76)$$

which has all atoms in the equal superposition of two internal states. Obviously, $|\Psi_{in}\rangle$ is a CSS of $\theta = \frac{\pi}{2}$ and $\varphi = 0$. Then, the system undergoes a free evolution for a period of time, in which the ground state $|\downarrow\rangle$ accumulates a phase $\varphi/2$ and the excited state $|\uparrow\rangle$ accumulates a phase $-\varphi/2$. At the end of the free evolution, the state reads as,

$$|\Psi_{out}\rangle = \otimes_{i=1}^N \left[\frac{1}{\sqrt{2}} \left(e^{-i\frac{\varphi}{2}} |\uparrow\rangle_i + e^{+i\frac{\varphi}{2}} |\downarrow\rangle_i \right) \right]. \quad (77)$$

Finally, the second $\frac{\pi}{2}$ pulse is applied and the accumulated relative phase is extracted from the mean population difference $\langle n_{\uparrow} - n_{\downarrow} \rangle = 2 \langle \hat{J}_z \rangle$.

The evolution from the initial state $|\Psi_0\rangle$ to the final state $|\Psi_f\rangle$ is described by

$$|\Psi_f\rangle = \hat{U} |\Psi_0\rangle, \quad (78)$$

with the propagation operator^{112,113}

$$\hat{U} = \exp\left(-i\frac{\pi}{2}\hat{J}_y\right) \exp\left(-i\varphi\hat{J}_z\right) \exp\left(-i\frac{\pi}{2}\hat{J}_y\right). \quad (79)$$

Therefore, the expectation value for the final state is given by

$$\langle \hat{J}_z \rangle_f = \langle \Psi_f | \hat{J}_z | \Psi_f \rangle = \langle \Psi_0 | \hat{U}^\dagger \hat{J}_z \hat{U} | \Psi_0 \rangle. \quad (80)$$

Substituting Eq. (79) into Eq. (80), we get

$$\langle \hat{J}_z \rangle_f = -\cos \varphi \langle \hat{J}_z \rangle_0 + \sin \varphi \langle \hat{J}_y \rangle_0, \quad (81)$$

and

$$\begin{aligned} (\Delta \hat{J}_z)_f^2 &= (\Delta \hat{J}_z)_0^2 \cos^2 \varphi + (\Delta \hat{J}_y)_0^2 \sin^2 \varphi \\ &\quad - \sin \varphi \cos \varphi \langle \hat{J}_z \hat{J}_y + \hat{J}_y \hat{J}_z \rangle. \end{aligned} \quad (82)$$

As the initial state $|\Psi_0\rangle = \otimes_{l=1}^N |\downarrow\rangle_l$, we have

$$\langle \hat{J}_z \rangle_0 = -\frac{N}{2}, (\Delta \hat{J}_z)_0 = 0, (\Delta \hat{J}_x)_0 = (\Delta \hat{J}_y)_0 = \frac{\sqrt{N}}{2}. \quad (83)$$

Thus the standard deviation of the final state reads as,

$$(\Delta \hat{J}_z)_f = \frac{\sqrt{N}}{2} \sin \varphi. \quad (84)$$

Applying Eq. (3), the standard deviation of φ is given as

$$\Delta \varphi = \frac{(\Delta \hat{J}_z)_f}{|\partial \langle \hat{J}_z \rangle_f / \partial \varphi|} = \frac{1}{\sqrt{N}}. \quad (85)$$

This means that the measurement precision for the Ramsey interferometry with CSS obeys the scaling imposed by the standard quantum limit.

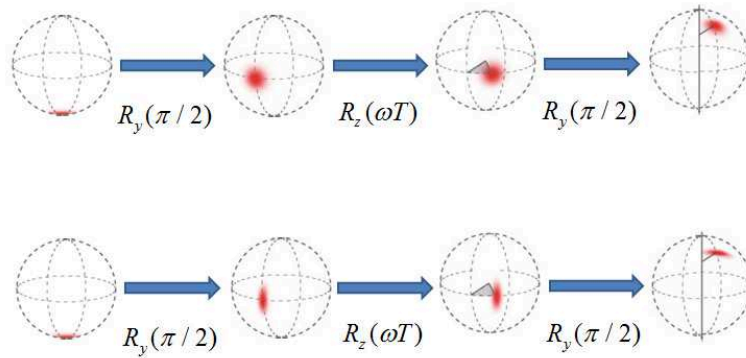


Fig. 4. Schematic diagrams of Ramsey interferometry on the Bloch sphere. Top: The initial state is a coherent spin state. Bottom: The initial state is a spin squeezed state. Adapted from Ref. 6.

4.2. Spin squeezed states

Similar to the quantum squeezing of position and momentum, without violating the Heisenberg uncertainty relation, the fluctuations of one spin

component can be reduced below the symmetric limit at the expense of the increased fluctuations of the other spin component. The state of reduced spin fluctuations along a specific direction is called spin squeezed state (SSS).^{114,115} The reduced spin fluctuations may be employed to increase the measurement precision. The occurrence of quantum spin squeezing relates to quantum entanglement among the particles.^{116–119}

There are several definitions for quantum spin squeezing.¹²⁰ The first squeezing parameter ξ_H is defined according to Heisenberg uncertainty relation.¹²¹ It can be expressed as

$$\xi_H^2 = \frac{2(\Delta\hat{J}_\alpha)^2}{|\langle\hat{J}_\gamma\rangle|}, \alpha \neq \gamma \in (x, y, z). \quad (86)$$

A state of $\xi_H^2 < 1$ is a spin squeezed state. The second squeezing parameter ξ_S is defined by the minimum fluctuation along the direction perpendicular to the MSD.¹²² It can be written as

$$\xi_S^2 = \frac{\min(\Delta\hat{J}_{\vec{n}_\perp})^2}{j/2} = \frac{4\min(\Delta\hat{J}_{\vec{n}_\perp})^2}{N}. \quad (87)$$

Here, the minimization over all possible directions \vec{n}_\perp is to find the most squeezed direction perpendicular to the MSD. The state is supposed to be squeezed if $\xi_S^2 < 1$. The third squeezing parameter ξ_R is defined by the ratio of the phase fluctuation for the considered state and a reference CSS.^{14,112,123} It reads as

$$\xi_R^2 = \frac{\Delta\phi}{(\Delta\phi)_{css}} = \frac{N(\Delta\hat{J}_{\vec{n}_\perp})^2}{|\langle\hat{J}\rangle|^2}. \quad (88)$$

This spin squeezing parameter is widely used in atomic Ramsey interferometry. In realistic experiments, $\Delta\hat{J}_{\vec{n}_\perp}$ can be obtained by measuring the population difference after an appropriate state rotation and $|\langle\hat{J}\rangle|$ can be extracted from the Ramsey fringes contrast. The state is spin squeezed if $\xi_R^2 < 1$. There are small differences among the definitions for the spin squeezing parameter. For an example, the differences between the definitions (83) and (84) are analyzed and the source of differences is explained by using the negativity criterion for entanglement.¹²⁴

It has demonstrated that the Ramsey interferometry with a SSS as the input state may have a higher measurement precision than the case of a CSS.¹²⁵ Here, we assume the initial state is a SSS of

$$\langle\hat{J}_y\rangle_0 = 0, \langle\hat{J}_z\rangle_0 = -\frac{N}{2}, (\Delta\hat{J}_y)_0 = \frac{\sqrt{N}}{2}\xi_R, \quad (89)$$

where the initial spin fluctuations are squeezed along the y -axis, i.e., the squeezing parameter $\xi_R < 1$.

Similar to the single-particle case, the interferometry with a SSS also includes two $\frac{\pi}{2}$ pulses and a free evolution. The first $\frac{\pi}{2}$ pulse rotates the initial SSS an angle $\frac{\pi}{2}$ around the y -axis. In the free evolution process, the state rotates around the z -axis with a unknown angle φ to be measured. Then applying the second $\frac{\pi}{2}$ pulse, the state rotates another $\frac{\pi}{2}$ around the y -axis. Finally, an additional rotation around its center is applied before measuring the population difference, which ensures the final population difference has minimal fluctuations.¹⁴

The evolution from the initial state to the final state can be written as

$$|\psi_f\rangle = \hat{U}|\psi_0\rangle, \quad (90)$$

with the propagation operator

$$\hat{U} = \exp(-i\frac{\pi}{2}\hat{S}_y) \exp(-i\varphi\hat{S}_z) \exp(-i\frac{\pi}{2}\hat{S}_y). \quad (91)$$

The expectation value of \hat{J}_z is given as

$$\langle \hat{J}_z \rangle_f = -\cos\varphi \langle \hat{J}_z \rangle_0 + \sin\varphi \langle \hat{J}_y \rangle_0, \quad (92)$$

and its variance reads as

$$\begin{aligned} (\Delta \hat{J}_z)_f^2 &= (\Delta \hat{J}_z)_0^2 \cos^2\varphi + (\Delta \hat{J}_y)_0^2 \sin^2\varphi \\ &\quad - \sin\varphi \cos\varphi \langle \hat{J}_z \hat{J}_y + \hat{J}_y \hat{J}_z \rangle. \end{aligned} \quad (93)$$

Obviously, the final state $|\psi_f\rangle$ is a SSS where the squeezed direction forms at an angle α relative to the \hat{J}_x axis. To read out \hat{J}_z with minimal uncertainty, one has to rotate the uncertainty ellipse of $|\psi_f\rangle$ around its center by an angle related to α . Therefore, without any change of the expectation value of \hat{J}_z , the readout variance of \hat{J}_z reads as

$$(\Delta \hat{J}_z)_{\text{readout}}^2 = (\Delta \hat{J}_y)_0^2. \quad (94)$$

which is given by the initial variance of \hat{J}_y . According to Eq. (3), the standard deviation of φ can be expressed as,

$$\Delta\varphi = \frac{(\Delta \hat{J}_z)_0}{|\partial \langle \hat{J}_z \rangle_f / \partial \varphi|} = \frac{\xi_R \sqrt{N}/2}{|\sin\varphi| N/2} = \frac{\xi_R}{|\sin\varphi| \sqrt{N}}. \quad (95)$$

Clearly, the measurement precision $\Delta\varphi$ reaches its minimum,

$$\Delta\varphi = \frac{\xi_R}{\sqrt{N}} \quad (96)$$

if $\varphi = \frac{\pi}{2}$. In comparison to coherent spin states, spin squeezed states may be used to beat the standard quantum limit: $\Delta\varphi \sim 1/\sqrt{N}$. For an example, if the initial state is squeezed to $\xi_R \sim 1/\sqrt{N}$, the best measurement precision can reach the Heisenberg limit: $\Delta\varphi \sim 1/N$.

4.3. NOON states

Theoretically, the NOON state has been proposed as one of the best candidates to improve the measurement precision. An NOON state is an equal-probability superposition of all N particles in mode a with zero particle in mode b , and vice versa. If the two modes are regarded as two possible paths for particles, the NOON state can be interpreted as all N particles pass through either path a or path b together, which is also called the path-entangled state.^{47,48,81,126} In general, it can be written in form of

$$|\text{NOON}\rangle = \frac{1}{\sqrt{2}} (|N\rangle_a |0\rangle_b + e^{i\theta} |0\rangle_a |N\rangle_b), \quad (97)$$

with θ denoting an arbitrary phase. The NOON state is equivalent to the N -particle GHZ state, which is the maximally entangled state for a multiparticle system of two-state particles.¹²⁷⁻¹²⁹ For a multiparticle system involving two single-particle states $|\downarrow\rangle$ and $|\uparrow\rangle$, the N -particle GHZ state can be expressed as

$$|\text{GHZ}\rangle = \frac{1}{\sqrt{2}} \left(\left| \frac{N}{2}, +\frac{N}{2} \right\rangle + e^{i\theta} \left| \frac{N}{2}, -\frac{N}{2} \right\rangle \right), \quad (98)$$

with the Dicke basis, $|J = \frac{N}{2}, m = \frac{1}{2}(n_\uparrow - n_\downarrow)\rangle$.

Below, we consider the Ramsey interferometry with,

$$|\Psi\rangle_{in} = \frac{1}{\sqrt{2}} \left(\left| \frac{N}{2}, +\frac{N}{2} \right\rangle + \left| \frac{N}{2}, -\frac{N}{2} \right\rangle \right), \quad (99)$$

as the input state before the free evolution. In the free evolution, because of the entanglement, all particles simultaneously acquire the phase shift and each particle contribute a phase shift $+\frac{\varphi}{2}$ (or $-\frac{\varphi}{2}$) corresponding to $|\downarrow\rangle$ (or $|\uparrow\rangle$). Therefore, after the free evolution, the state reads as

$$|\Psi\rangle_{out} = \frac{1}{\sqrt{2}} \left(e^{-i\frac{N\varphi}{2}} \left| \frac{N}{2}, +\frac{N}{2} \right\rangle + e^{+i\frac{N\varphi}{2}} \left| \frac{N}{2}, -\frac{N}{2} \right\rangle \right). \quad (100)$$

Below, we employ the quantum Fisher information to analyze the minimal uncertainty of measuring the phase φ . By differentiating the output state $|\Psi\rangle_{out}$ with respect to the relative phase φ , we have

$$\frac{d|\Psi\rangle_{out}}{d\varphi} = -\frac{iN}{2\sqrt{2}} \left(e^{-i\frac{N\varphi}{2}} \left| \frac{N}{2}, +\frac{N}{2} \right\rangle - e^{+i\frac{N\varphi}{2}} \left| \frac{N}{2}, -\frac{N}{2} \right\rangle \right). \quad (101)$$

According to Eq. (41), the quantum Fisher information is given as

$$F_Q^N = 4 \left[\langle \psi'(\varphi) | \psi'(\varphi) \rangle - |\langle \psi'(\varphi) | \psi(\varphi) \rangle|^2 \right] = 4 \left(\frac{N^2}{4} - 0 \right) = N^2. \quad (102)$$

Therefore, the phase uncertainty satisfies,

$$\Delta\varphi \geq \frac{1}{F_Q} = \frac{1}{N}, \quad (103)$$

which is the scaling of the Heisenberg limit. In comparison to the case of independent particles, the measurement precision is improved from the standard quantum limit to the Heisenberg limit.⁹¹ However, in realistic experiments, it is hard to prepare a large-N GHZ state and the GHZ state is fragile in the presence of particle losses.¹³⁰

4.4. Entangled coherent states

An entangled coherent state (ECS) is a superposition of multimode coherent states.^{131,132} A typical class of the ECS is defined as,¹³³

$$\begin{aligned} |\text{ECS}\rangle &= e^{(-|\alpha|^2)/2} N_\alpha \sum_{n=0}^{\infty} \frac{\alpha^n}{n!} \left[(\hat{a}^\dagger)^n + (\hat{b}^\dagger)^n \right] |0\rangle_a |0\rangle_b \\ &= N_\alpha [|\alpha\rangle_a |0\rangle_b + |0\rangle_a |\alpha\rangle_b], \end{aligned} \quad (104)$$

with the normalization factor $N_\alpha = 1/\sqrt{2(1 + e^{-|\alpha|^2})}$. This ECS can be understood as the superposition of multiple NOON states with different total particle numbers. As a coherent state involves Fock states with particle number from zero to infinity, the averaged total particle number but not the total particle number itself is a good quantity. The averaged total particle number of the ECS (104) is given by

$$\langle n \rangle = \langle n_a + n_b \rangle = 2N_\alpha^2 |\alpha|^2. \quad (105)$$

Let us consider a Mach-Zehnder interferometry with the ECS (104) as the input state for free propagation and the two modes a and b as two paths. Here, we assume that each particle in mode b acquires a phase shift φ with respect to the one in mode a . That is, the state after the free propagation reads as

$$\begin{aligned} |\Psi\rangle_{out} &= N_\alpha e^{-\frac{|\alpha|^2}{2}} \sum_{n=0}^{\infty} \frac{\alpha^n}{n!} \left[(\hat{a}^\dagger)^n + (\hat{b}^\dagger)^n e^{in\varphi} \right] |0\rangle_a |0\rangle_b \\ &= N_\alpha e^{-\frac{|\alpha|^2}{2}} \left[\left(\sum_{n=0}^{\infty} \frac{\alpha^n}{\sqrt{n!}} |n\rangle_a \right) |0\rangle_b + \left(\sum_{n=0}^{\infty} \frac{\alpha^n}{\sqrt{n!}} e^{in\varphi} |n\rangle_b \right) |0\rangle_a \right] \end{aligned} \quad (106)$$

Therefore, the derivative of the output state $|\Psi\rangle_{out}$ with respect to φ reads as

$$\frac{d|\Psi\rangle_{out}}{d\varphi} = N_\alpha \left[|0\rangle_a \left(e^{-\frac{|\alpha|^2}{2}} \sum_{n=0}^{\infty} \frac{i n \alpha^n}{\sqrt{n!}} e^{in\varphi} |n\rangle_b \right) \right]. \quad (107)$$

According to Eq. (41), the quantum Fisher information is given by

$$F_Q = 4 |\alpha|^2 N_\alpha^2 + 4(1 - N_\alpha^2) |\alpha|^4 N_\alpha^2. \quad (108)$$

Thus the phase uncertainty $\Delta\varphi$ satisfies

$$\Delta\varphi \geq \frac{1}{2 |\alpha| N_\alpha \sqrt{1 + (1 - N_\alpha^2) |\alpha|^2}}. \quad (109)$$

If the parameters satisfy the conditions of $\alpha \gg 1$, $N_\alpha \approx 1/\sqrt{2}$ and $|\alpha|^2 \approx \langle n \rangle \gg 1$, the phase uncertainty obeys

$$\Delta\varphi \geq \frac{1}{\sqrt{2\langle n \rangle} \sqrt{1 + \langle n \rangle/2}} \approx \frac{1}{\langle n \rangle}. \quad (110)$$

This means that the phase uncertainty can approach to the Heisenberg limit.

4.5. Twin Fock states

The twin Fock state,

$$|\text{TWIN}\rangle = |N\rangle_a |N\rangle_b, \quad (111)$$

is a two-mode Fock state with equal particle number for the two modes. By using the twin Fock states as input states and parity measurements, it has been demonstrated the Heisenberg-limited Mach-Zehnder interferometry.^{96,102,134,135}

The first beam splitter transforms the twin Fock state into

$$|\Psi\rangle_{BS1} = U_{BS1} |\text{TWIN}\rangle = \sum_{k=0}^N C_k^N |2k\rangle_a |2N - 2k\rangle_b, \quad (112)$$

with the beam splitter operator,

$$\hat{U}_{BS1} = \exp \left[\frac{\pi}{4} (\hat{a}^\dagger \hat{b} - \hat{b}^\dagger \hat{a}) \right], \quad (113)$$

and the coefficients,

$$C_k^N = \frac{1}{2^N} (-1)^{N-k} \left[\binom{2k}{k} \binom{2N-2k}{N-k} \right]^{1/2}. \quad (114)$$

Here \hat{a} and \hat{b} are the two annihilation operators for particles in modes a and b , respectively. A free propagation follows the first beam splitter, in which each particles in mode b accumulates a relative phase φ . Therefore, after the free propagation, the state reads as

$$|\Psi(\varphi)\rangle = \sum_{k=0}^N e^{i\varphi(2N-2k)} C_k^N |2k\rangle_a |2N-2k\rangle_b, \quad (115)$$

which includes the information of the phase φ to be measured. Then the second beam splitter,

$$\hat{U}_{BS2} = \exp\left[-i\frac{\pi}{4}(\hat{a}^\dagger\hat{b} + \hat{b}^\dagger\hat{a})\right], \quad (116)$$

is applied to $|\Psi(\varphi)\rangle$ and the state becomes

$$|\Psi\rangle_{out} = \hat{U}_{BS2}|\Psi(\varphi)\rangle. \quad (117)$$

At last, a parity measurement is performed for one of two modes. Parity measurements have been widely used to extract phase shifts in quantum optical metrology¹³⁶ with highly entangled states including NOON states, entangled coherent states and twin Fock states. Further, the parity measurement has been adapted to extract the relative phase between Bose condensed atoms in different hyperfine levels.¹³⁷

Here, the parity operator of mode b can be expressed as

$$\hat{\Pi}_b = \exp(i\pi\hat{b}^\dagger\hat{b}), \quad (118)$$

and its expectation value is a Legendre polynomial,

$$\langle\hat{\Pi}_b\rangle = \langle\Psi|\hat{\Pi}_b|\Psi\rangle_{out} = \langle\Psi(\varphi)|\hat{U}_{BS2}^\dagger\hat{\Pi}_b\hat{U}_{BS2}|\Psi(\varphi)\rangle = P_N[\cos(2\varphi)]. \quad (119)$$

According to Eq. (3), the phase uncertainty is given by

$$\Delta\varphi = \frac{\Delta\hat{\Pi}_b}{\left|\partial\langle\hat{\Pi}_b\rangle/\partial\varphi\right|}. \quad (120)$$

For $\varphi \rightarrow 0$, the phase uncertainty $\Delta\varphi$ versus the particle number N approaches to the Heisenberg limit $\Delta\varphi_{HL} = 1/(2N)$. For other values of φ , the phase uncertainty $\Delta\varphi$ will blow up for some specific values of the total particle number and it still approaches to the Heisenberg limit for the other values of the total particle number.

The phase uncertainty can also be derived by calculating the quantum Fisher information. The derivative of $|\Psi(\varphi)\rangle$ with respect to φ reads as

$$\frac{d|\Psi(\varphi)\rangle}{d\varphi} = \sum_{k=0}^N i(2N - 2k)e^{i\varphi(2N-2k)} C_k^N |2k\rangle_a |2N - 2k\rangle_b. \quad (121)$$

Substituting this derivative into Eq. (41), we obtain the quantum Fisher information,

$$F_Q = 2N(1 + N). \quad (122)$$

Thus the quantum Cramér-Rao bound for the phase uncertainty is given as

$$\Delta\varphi \geq \frac{1}{\sqrt{2N^2 + 2N}}, \quad (123)$$

which indicates that the minimal phase uncertainty obtained by the optimal measurement can reach the Heisenberg limit. This bound is consistent with the phase uncertainty obtained by the parity measurement.

5. Experimental Progresses

In recent years, there appear great advances in quantum metrology with multiparticle systems. In particular, multiparticle entangled states have been widely used to implement high-precision metrology from spectroscopy, interferometers to atomic clocks.^{138–142} To implement high-precision metrology with entangled multiparticle systems, in addition to the similar operations in quantum metrology with independent particles, a key problem is how to generate multiparticle entanglement. Usually, the multiparticle entanglement can be generated by intrinsic or artificial inter-particle interactions, such as, the intrinsic s-wave scattering between ultracold atoms, the Coulomb interaction between ultracold trapped ions, the laser-induced interaction and the continuous quantum non-demolition measurement. Below, we briefly review some typical progresses in quantum metrology with Bose-Einstein condensed atoms,^{6,7,10} ultracold trapped ions^{143,144} and cold atomic ensembles.^{8,9}

5.1. Bose-Einstein condensed atoms

An atomic Bose-Einstein condensate (BEC) has intrinsic atom-atom interaction dominated by the s-wave scattering, which can be used to generate entangled states such as spin squeezed states,^{145–150} GHZ states¹⁵¹ and twin

Fock states.^{102,135} In recent experiments, the spin squeezed states have been generated by one-axis twisting and then they are used to implement high-precision interferometry beyond the standard quantum limit.^{6,7,18,122,152,153} It has also been demonstrated the generation of twin Fock states via spin dynamics and the applications of the generated twin Fock states in high-precision interferometers.¹⁰ Different from the schemes with distinguishable particles, which need entangled input states for beating the standard quantum limit, the schemes with identical Bose condensed atoms do not need entangled input states^{154–156} and the entanglement can be dynamically generated in these schemes via time evolution.^{6,7}

5.1.1. Nonlinear interferometry with spin squeezed states

Generally speaking, due to the intrinsic nonlinear interaction between atoms, almost all interferometers with Bose condensed atoms are nonlinear. Most of the interferometers with atomic BECs can be described by Bose-Josephson Hamiltonians. Here, for simplicity, we only discuss Bose-Josephson systems^{16,25,157–173} of Bose-Einstein condensed atoms in two different modes. There are two typical Bose-Josephson systems. One is the external Bose-Josephson junction (BJJ), which is realized by an atomic BEC in a deep double-well potential. The other is the internal BJJ, which is realized by Bose-Einstein condensed atoms involving two coupled hyperfine states. There are lots of studies on macroscopic quantum phenomena in BJJs. Here, we concentrate our discussions on many-body quantum interferometry with quantized BJJs.

In second quantization, the external BJJ can be described by the many-body Hamiltonian,

$$H = \int d\mathbf{r} \hat{\Psi}^\dagger(\mathbf{r}) \left[-\frac{\hbar^2 \nabla^2}{2m} + V_{dw}(\mathbf{r}) \right] \hat{\Psi}(\mathbf{r}) + \frac{g}{2} \int d\mathbf{r} \hat{\Psi}^\dagger(\mathbf{r}) \hat{\Psi}^\dagger(\mathbf{r}) \hat{\Psi}(\mathbf{r}) \hat{\Psi}(\mathbf{r}), \quad (124)$$

where $\hat{\Psi}(\mathbf{r})$ and $\hat{\Psi}^\dagger(\mathbf{r})$ are bosonic field operators, $V_{dw}(\mathbf{r})$ is the double-well potential, $g = 4\pi\hbar a_s/m$, and a_s is the s-wave scattering length. By applying the two-mode approximation,¹⁷³ the field operator reads as,

$$\hat{\Psi}(\mathbf{r}) = \hat{b}_1 \phi_1(\mathbf{r}) + \hat{b}_2 \phi_2(\mathbf{r}), \quad (125)$$

with \hat{b}_1 and \hat{b}_2 represent the Bose annihilation operators for the atoms in the Wannier states $\phi_1(\mathbf{r})$ and $\phi_2(\mathbf{r})$, respectively.

While for an internal BJJ, it obeys the many-body quantum Hamiltonian,

$$H = \int d\mathbf{r} \left(\hat{\Psi}_1^\dagger(\mathbf{r}), \hat{\Psi}_2^\dagger(\mathbf{r}) \right) \begin{pmatrix} h_1^{(0)} & -\frac{\hbar\Omega}{2} \\ -\frac{\hbar\Omega}{2} & h_2^{(0)} \end{pmatrix} \begin{pmatrix} \hat{\Psi}_1(\mathbf{r}) \\ \hat{\Psi}_2(\mathbf{r}) \end{pmatrix} + H_{int}, \quad (126)$$

with

$$h_1^{(0)} = -\frac{\hbar^2 \nabla^2}{2m} + V_1(\mathbf{r}) - \frac{\Delta}{2},$$

$$h_2^{(0)} = -\frac{\hbar^2 \nabla^2}{2m} + V_2(\mathbf{r}) + \frac{\Delta}{2},$$

and

$$H_{int} = H_{11} + H_{22} + H_{12},$$

$$H_{11} = \frac{g_{11}}{2} \int d\mathbf{r} \hat{\Psi}_1^\dagger(\mathbf{r}) \hat{\Psi}_1^\dagger(\mathbf{r}) \Psi_1(\mathbf{r}) \hat{\Psi}_1(\mathbf{r}),$$

$$H_{22} = \frac{g_{22}}{2} \int d\mathbf{r} \hat{\Psi}_2^\dagger(\mathbf{r}) \hat{\Psi}_2^\dagger(\mathbf{r}) \Psi_2(\mathbf{r}) \hat{\Psi}_2(\mathbf{r}),$$

$$H_{12} = \frac{g_{12}}{2} \int d\mathbf{r} \hat{\Psi}_2^\dagger(\mathbf{r}) \hat{\Psi}_1^\dagger(\mathbf{r}) \Psi_1(\mathbf{r}) \hat{\Psi}_2(\mathbf{r}).$$

Here, Ω is the Rabi frequency of the coupling, Δ is the detuning to resonance, $V_j(\mathbf{r})$ denote the trapping potentials, and g_{ij} describe the s-wave scattering of atoms in modes i and j . For a spin-independent trap $V_1(\mathbf{r}) = V_2(\mathbf{r})$, assuming all atoms staying in the same spatial state $\phi(\mathbf{r})$, we can apply the two-mode approximation,

$$\hat{\Psi}_j(\mathbf{r}) = \hat{b}_j \phi(\mathbf{r}), \quad (j = 1 \text{ and } 2), \quad (127)$$

with \hat{b}_1 and \hat{b}_2 being the annihilation operators for the atoms in the two hyperfine states.

By integrating the spatial coordinates, both external and internal BJJs can be described by a unified two-mode Bose-Hubbard model,²⁵

$$H = -\frac{J}{2} \left(\hat{b}_2^\dagger \hat{b}_1 + \hat{b}_1^\dagger \hat{b}_2 \right) + \frac{\delta}{2} (\hat{n}_2 - \hat{n}_1) + \frac{E_c}{8} (\hat{n}_2 - \hat{n}_1)^2, \quad (128)$$

where J is the tunneling strength, δ is the imbalance and E_c is the effective “charging” energy. For an external BJJ, $E_c \propto g$. While for an internal BJJ, $E_c \propto g_{11} + g_{22} - 2g_{12}$. Obviously, $[\hat{N}, H] = 0$, therefore the total atomic number $\hat{N} = \hat{b}_1^\dagger \hat{b}_1 + \hat{b}_2^\dagger \hat{b}_2$ is conserved. By using the Fock basis $\{|n_1, n_2\rangle\}$, an arbitrary state can be expressed as $|\Psi\rangle = \sum_{n_1, n_2} C_{n_1 n_2} |n_1, n_2\rangle$, where $n_j = \hat{b}_j^\dagger \hat{b}_j$ are the number of particles in the j -th mode.

Ground state and quasi-particle excitations of the BJJ Hamiltonian (128) sensitively depend on the ratio between the tunneling strength J and the charging energy E_c .^{163,165,166,168} The competition between the Josephson tunneling and the nonlinear interaction results different ground-state behaviors. For a symmetric BJJ ($\delta = 0$), dependent on the ratio $|E_c/J|$, the system shows three different regimes: Rabi, Fock and Josephson regimes.¹⁶⁵

- **(a) Rabi regime**, $|E_c/J| \ll N^{-1}$, in which the system is dominated by the Josephson term of J and there is a well defined relative phase between the two modes. The ground state is a coherent spin state, $|CSS\rangle = \exp(i\varphi\hat{J}_z) \exp(i\theta\hat{J}_y)|N/2, +N/2\rangle$.
- **(b) Fock regime**, $|E_c/J| \gg N$, in which the system is dominated by the nonlinear interaction term of E_c and the relative phase between the two modes is completely random. The ground state depends on the sign of the nonlinear interaction term. If E_c is positive, the ground state is a single Fock state $|\frac{N}{2}, \frac{N}{2}\rangle$ for even N or a superposition of two Fock states $\frac{1}{\sqrt{2}}(|\frac{N}{2}, -1\rangle + |\frac{N}{2}, 1\rangle)$ for odd N . If E_c is negative, there are two degenerate ground states $|\frac{N}{2}, \frac{N}{2}\rangle$ and $|\frac{N}{2}, -\frac{N}{2}\rangle$. Therefore, any superposition of these two degenerated states including the GHZ state $\frac{1}{\sqrt{2}}(|\frac{N}{2}, \frac{N}{2}\rangle + |\frac{N}{2}, -\frac{N}{2}\rangle)$ is also a ground state. It has been proposed that the GHZ state can be adiabatically prepared and then it can be used to achieve a Heisenberg-limited interferometry.¹⁶
- **(c) Josephson regime**, $N^{-1} \ll |E_c/J| \ll N$, in which the number imbalance and the relative phase are both fluctuating and the ground state is an intermediate squeezed state.

In terms of the collective spin operators (64), (65) and (66), the BJJ Hamiltonian (128) becomes as

$$H = -B_x\hat{J}_x + B_z\hat{J}_z + \chi\hat{J}_z^2, \quad (129)$$

where the transverse magnetic field $B_x = 2J$, the longitudinal magnetic field $B_z = \delta$ and the nonlinear interaction energy $\chi = \frac{E_c}{2}$. This Hamiltonian is just the ‘one-axis twisting’ Hamiltonian for generating quantum spin squeezing.¹²² In recent, several theoretical methods for generating spin squeezed states in BJJs have been proposed.^{174–177} In realistic systems of Bose condensed atoms, thermal atoms and atom loss have significant effects on the achievable optimal spin squeezing.^{111,178–180}

Dramatic observations of phase fluctuations and number squeezing in external BJJs have been made. The phase fluctuations were observed by Gati et al.,¹⁸¹ Jo et al.¹⁸² and Hofferberth et al.^{183,184} The number squeezing was observed by Jo et al.¹⁸⁵ and Esteve et al.¹⁸⁶ In addition, for an array of independent BECs, the phase fluctuations were observed by Hadzibabic et al.¹⁸⁷ and the number squeezing was observed by Orzel et al.¹⁸⁸ Moreover, the achieved squeezing in external BJJs, a kind of multiparticle entanglement, can be used to implement precision metrology with spatial atom interferometers.¹⁸⁶

The spin squeezing in internal BJJs and the use of the prepared spin squeezed states in precision metrology have also been demonstrated. Generally, the inter-mode coupling for an internal BJJ should be characterized by a Rabi frequency Ω , a phase γ and a detuning δ , therefore the internal BJJ obeys the one-axis twisting Hamiltonian

$$H = \Omega \hat{J}_\gamma + \delta \hat{J}_z + \chi \hat{J}_z^2, \quad (130)$$

with $\hat{J}_\gamma = (\cos \gamma) \hat{J}_x - (\sin \gamma) \hat{J}_y$. Described by this Hamiltonian, the spin squeezing of Bose condensed atoms has been demonstrated by two experimental groups: Oberthaler's group and Treutlein's group. They independently developed two different methods for turning on the strongly nonlinear interactions and then generating quantum spin squeezing. Oberthaler's group has used the Feshbach resonance to decrease the inter-component s-wave scattering length.⁶ Taking into account the technical noises, the squeezing factor in this experiment⁶ can reach $\xi_N^2 = -8.2_{-1.2}^{+0.8}$ dB, which is close to the atom-loss-limited theoretical optimum for this system. Treutlein's group has used a state-dependent trap to decrease the density overlap between two components.⁷ To obtain the best squeezing angle in their experiments, they measured the squeezing factor for different rotation angle.

(a) *The experiment with optical lattices*

By loading Bose condensed atoms into optical lattices, Oberthaler's group has successfully prepared the entanglement of about 170 ^{87}Rb atoms and then realized a nonlinear Ramsey interferometer.⁶ In comparison to the ideal phase sensitivity obtained by unentangled states, their experimental data show that the phase sensitivity is enhanced by 15 percent. They firstly prepare a BEC of ^{87}Rb atoms occupying the hyperfine state $|F = 1, m_F = -1\rangle$ in an optical dipole trap. Then, through supposing a one-dimensional optical lattice potential, the dipole trap splits into six, which

allows to perform six independent experiments in parallel. Before applying the first $\frac{\pi}{2}$ pulse, the atoms are swept from the state $|F = 1, m_F = -1\rangle$ to the state $|a\rangle = |F = 1, m_F = 1\rangle$. Since the first $\frac{\pi}{2}$ pulse, only two hyperfine states $|a\rangle = |F = 1, m_F = 1\rangle$ and $|b\rangle = |F = 2, m_F = -1\rangle$ are involved and individual systems localized in each lattice site can be described by the one-axis twisting Hamiltonian. The effective nonlinear interaction $\chi \propto a_{aa} + a_{bb} - 2a_{ab}$ relates to the intra-species and inter-species interactions. The inter-species interaction is tuned by the Feshbach resonance and $\chi = 2\pi \times 0.063$ Hz at a magnetic field of $B = 9.10$ G. The Rabi frequency Ω can be switched rapidly from 0 to $2\pi \times 600$ Hz. Therefore, the system can be adjusted between Rabi regime and Fock regime.

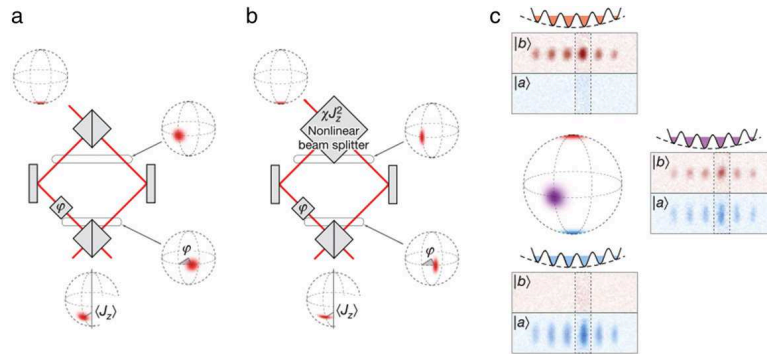


Fig. 5. (a) Schematic of a classical linear interferometer. (b) Schematic of a nonlinear interferometer. (c) Six independent BECs of ^{87}Rb in a one-dimensional optical lattice. Two-state atoms in each well form a two-mode system described by the one-axis twisting Hamiltonian. The individual detection of the condensate in each well can be achieved by high-intensity absorption imaging. From Ref. 6.

The input state for the interferometer is a coherent spin state polarized to the \hat{J}_z -direction. After the first $\pi/2$ pulse, the state rotates to the \hat{J}_x -direction, with $\langle J_z \rangle = \langle J_y \rangle = 0$ and $\Delta J_z = \Delta J_y = \sqrt{N}/2$. Then the Josephson coupling (ΩJ_γ) is switched off, the system stays in the Fock regime and its state evolves under the nonlinear term, which induces a squeezing angle α_0 with respect to z-direction. A rotation of the uncertainty ellipse around its center by $\alpha = \alpha_0 + \pi/2$ is followed. Then the modes $|a\rangle$ and $|b\rangle$ experience a $\tau = 2\mu\text{s}$ phase accumulation time and recombine via another $\pi/2$ pulse before the readout of population imbalance.

(b) The experiment with an atomic chip

By loading Bose condensed atoms into an atomic chip, Treutlein's group has created spin-squeezed states which may improve the measurement precision beyond the standard quantum limit.⁷ In the experiment, two spin states $|F = 1, m_F = -1\rangle$ and $|F = 2, m_F = 1\rangle$ of ^{87}Rb atoms are involved and the system obeys the one-axis twisting Hamiltonian (130). The effective inter-component interaction is controlled by adjusting the spatial overlap between two spin components.

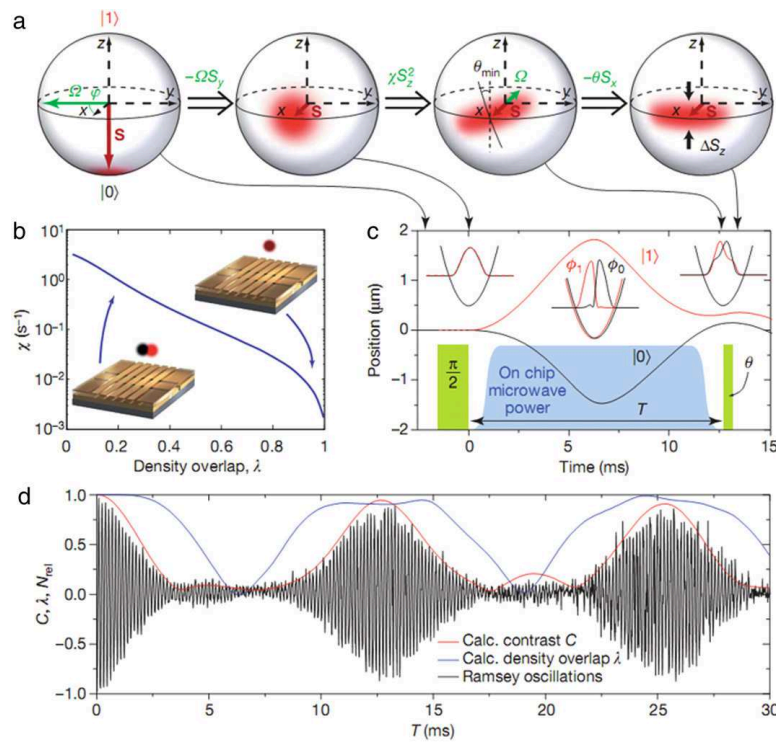


Fig. 6. (a) The preparation of spin squeezing on the generalized Bloch sphere. (b) The nonlinearity χ is decreased as the increase of the normalized density overlap λ of the two spin components. (c) The experimental sequence and the motion of two spin components corresponding to (a). (d) Measured Ramsey fringes in the normalized population difference N_{rel} . From Ref. 7.

To prepare spin squeezing, except for controlling the nonlinear interaction, Treutlein's group has used similar procedures in the experiment of

Oberthaler's group. First, a coherent spin state is prepared by a resonant $\frac{\pi}{2}$ pulse for 120 μs . During the pulse, the coupling term dominates, $\Omega \gg \chi N$, so that the atom-atom interaction can be neglected. The state-dependent microwave potential is turned on within 50 μs to cause a sudden separation of trap minima for the two hyperfine states. The two components begin to oscillate oppositely, the overlap of the modes wavefunction reduces, which leads to the decreasing of the inter-component interaction and the increasing of effective nonlinearity χ . The nonlinearity can attain $\chi = 1.5 s^{-1}$ at the maximum separation. The two components overlap again after 12.7 ms and the nonlinear interaction squeezing dynamics stops.

5.1.2. *Twin matter-wave interferometry*

In addition to the quantum interferometry with spin-squeezed states, twin matter-wave interferometry with initial twin Fock states has been demonstrated in experiment.¹⁰ Different the spin squeezing via one-axis twisting, spin exchange dynamics of Bose condensed atoms¹⁸⁹ has been used to create large ensembles of up to 10^4 pair-correlated atoms from initial twin Fock states. Attribute the pair correlation induced by spin exchange, the phase uncertainty can be beaten the standard quantum limit.

The experiment starts with creating a ^{87}Rb condensate of 2.8×10^4 atoms in the hyperfine state $|F = 2, m_F = 0\rangle$ in an optical dipole trap. Then the spin-exchange collision gradually produces correlated pairs of atoms with spins up and down. The functionality of the spin-exchange collision is just like a parametric amplifier, where the total number of the correlated pairs of atoms in $|F = 2, m_F = \pm 1\rangle$ increase exponentially with time. Afterwards, the trap is switched off and the three hyperfine states are split by a strong magnetic field gradient, and all three hyperfine states are recorded by absorption imaging. As the hyperfine states $|F = 2, m_F = \pm 1\rangle$ are generated in pairs, the number of particles in these two modes is exactly equal. Therefore, the twin Fock state is created with zero number difference and relative phase completely undetermined between these two modes.

Then the generated twin Fock state is input for implementing interferometry. The beam splitter of the interferometer is realized by three resonant microwave pulses. The first one is applied to transfer the atoms in $|F = 2, m_F = -1\rangle$ to $|F = 1, m_F = 0\rangle$. The second pulse with duration τ couples the states $|F = 1, m_F = 0\rangle$ and $|F = 2, m_F = 1\rangle$. The third pulse transfers the atoms from $|F = 1, m_F = 0\rangle$ to $|F = 2, m_F = -1\rangle$. The action of these three pulses is equivalent to a rotation around the x -axis by

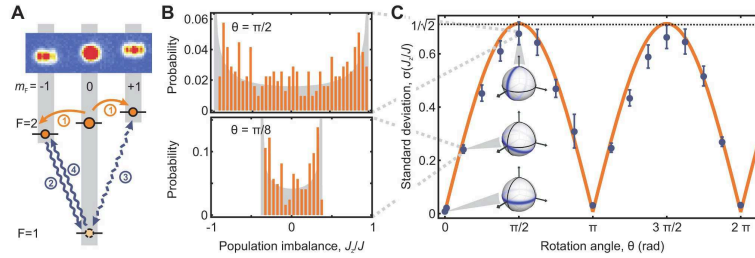


Fig. 7. (A) Schematic of the sequence of the realization of the beam splitter. Three microwave pulses are sequentially applied to achieve the coupling of the two hyperfine states $|F = 2, m_F = \pm 1\rangle$. The total effect is equivalent to a rotation around the x -axis by an angle θ . (B) Distribution of the normalized population difference for two different θ . The strongest fluctuations are obtained for $\theta = \frac{\pi}{2}$. The shaded area is the theoretical result. (C) The fluctuation of the normalized population difference versus the rotation angle θ , where the standard deviation $\sigma(J_z/J)$ oscillates approximately as $\sigma(J_z/J) = |\sin \theta|/\sqrt{2}$. From Ref. 10.

an angle $\theta = \tau\Omega_R$, where Ω_R is the Rabi frequency and τ is the duration of the coupling pulse. For $\theta = \frac{\pi}{2}$, the fluctuation of the population imbalance is maximal and it corresponds to the $\pi/2$ pulse in a Ramsey interferometer or the 50:50 beam splitter in a Mach-Zehnder interferometer.

It has been demonstrated that the phase uncertainty can be enhanced beyond the standard quantum limit. The phase uncertainty $\Delta\varphi$ is inferred from the state's sensitivity to small rotation around an arbitrary axis in the xy -plane. When $\varphi \approx 0.015$ rad, the phase uncertainty can reduce to $-1.61_{-1.1}^{+0.98}$ dB, which is below the shot noise limit. If taking into account both shot noise and detection noise, the phase uncertainty can be improved to $-2.5_{-1.1}^{+0.98}$ dB.

5.2. Ultracold trapped ions

Systems of ultracold atomic ions in a Paul trap provide an excellent platform for manipulating both the internal spin and external motional degrees of freedom. Ultracold trapped ions have been proposed to explore fundamental quantum principle and implement quantum information processing,^{85,190–197} quantum simulation^{198,199} and quantum metrology.^{24,30,85,143,144,200} Here, we give a brief introduction for some typical experiments of quantum metrology via ultracold trapped ions.

In 2001, Meyer et al. experimentally demonstrated that the sensitivity of rotation angle estimation with a Ramsey spectroscopy can be improved by using entangled trapped ions.¹⁴³ The experiment used two

${}^9\text{Be}^+$ ions that are confined in a linear radio-frequency trap. Two hyperfine states $|F = 1, m_F = -1\rangle \equiv |\uparrow\rangle$ and $|F = 2, m_F = -2\rangle \equiv |\downarrow\rangle$ form the basis of an effective spin-1/2 system. $|\uparrow\rangle$ and $|\downarrow\rangle$ are coupled by two-photon Raman transitions. The detection of the ions in states $|\uparrow\rangle$ and $|\downarrow\rangle$ is done by state-sensitive fluorescence. The use of entangled states for parity measurement and Ramsey spectroscopy has been demonstrated with $|\Psi_P\rangle = (e^{i\phi}|\uparrow\uparrow\rangle + |\downarrow\downarrow\rangle)/\sqrt{2}$ and $|\Psi_R\rangle = (|\uparrow\downarrow\rangle + |\downarrow\uparrow\rangle)/\sqrt{2}$, respectively. The experimental data show the measurement sensitivity is improved beyond the standard quantum limit (SQL) and close to the Heisenberg limit (HL).

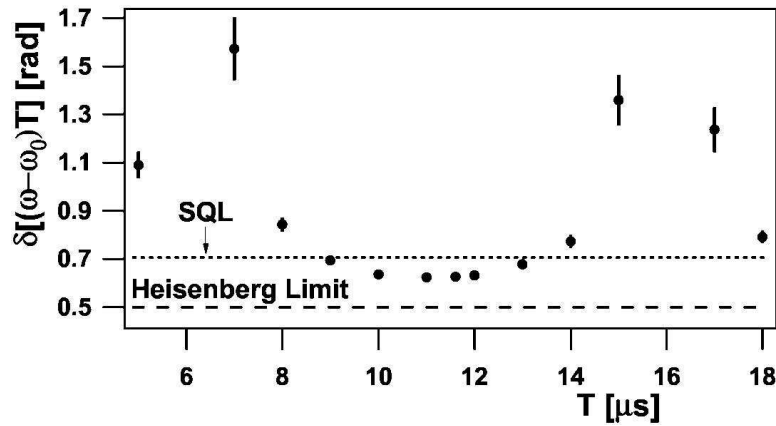


Fig. 8. Measurement precision in a Ramsey experiment with the initial state $|\Psi_R\rangle = (|\uparrow\downarrow\rangle + |\downarrow\uparrow\rangle)/\sqrt{2}$. The dotted line represent the SQL for two ions in a CSS. The dashed line is the Heisenberg limit. From Ref. 143.

In 2004, Leibfried et al. demonstrated the Ramsey spectroscopy with three entangled ${}^9\text{Be}^+$ ions in the GHZ state. The experimental data shows that the spectroscopic sensitivity is 1.45(2) times as high as that of a perfect experiment with three independent ions, which approaches the Heisenberg limit.¹⁴⁴

In 2006, Roos et al. demonstrated precision spectroscopy of a pair of trapped Ca^+ ions in a decoherence-free subspace of specifically designed entangled states.³⁰ In addition to the enhancement of signal-to-noise ratio in frequency measurements, a suitably designed pair of ions enable atomic clock measurements in the presence of magnetic field noise.

There are lots of experiments about the use of trapped atomic ions in

quantum metrology. More information of this field can be found in a review of Wineland and Leibfried.²⁰¹

5.3. Cold atomic ensembles

In addition to the realistic inter-particle interaction, quantum non-demolition (QND) has been widely used to generate quantum spin squeezing and entanglement.^{8,9,41,202–206} It has been demonstrated that the quantum spin squeezing and entanglement for over 100 thousand cold Cs atoms can be achieved by QND measurement on the atom clock levels.^{8,9} In the experiment, the two hyperfine states $|\uparrow\rangle \equiv |F = 4, m_F = 0\rangle$ and $|\downarrow\rangle \equiv |F = 3, m_F = 0\rangle$ of Cs atoms are referred to clock levels.

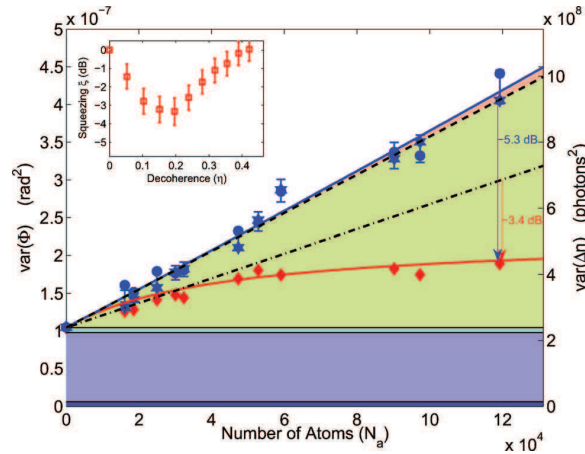


Fig. 9. Projection noise and spin squeezing via QND. Blue points, stars: variances $\text{Var}(\phi_1)$, $\text{Var}(\phi_2)$ of J_z of atoms in a CSS versus N_A ; solid blue line: quadratic fit; dashed line: CSS projection noise; red diamonds: conditionally reduced variance of a second J_z measurement predicted by the first variance; red line: reduced noise of SSS predicted from quadratic fits to projection noise data. Blue area, optical shot noise (light blue) and detector noise (dark blue); green area, projection noise. From Ref. 9.

The experiment is implemented as follows. Initially, by using optical pumping, the Cs atoms are prepared in the clock state $|\downarrow\rangle$. To prepare the CSS, a resonant $\pi/2$ microwave pulse at the clock frequency is applied. Then, successive QND measurements of the population difference $N_\uparrow - N_\downarrow$ are performed by measuring the state dependent phase shift of the off-resonant probe light in a balanced homodyne configuration. After the QND measurement, all atoms are pumped into the $F = 4$ level to determine the

total atom number N_A . Two identical linear polarized beam P_\uparrow and P_\downarrow off-resonantly probe the transitions $|F = 3\rangle$ to $|F' = 4\rangle$ and $|F = 4\rangle$ to $|F' = 5\rangle$, respectively. Each beam gains a phase shift proportional to the number of atoms in the corresponding clock states,

$$\phi_\uparrow = k_\uparrow N_\uparrow, \phi_\downarrow = k_\downarrow N_\downarrow,$$

where $k_{\uparrow(\downarrow)}$ are the coupling constants and the detuning $\Delta_{\uparrow(\downarrow)}$ are tuned to make $k_\uparrow = k_\downarrow = k$. The phase difference between the two arms of the Mach-Zehnder interferometer is related to the measurement of J_z and the shot noise of the photons,

$$\phi = \frac{\delta n}{n} + 2kJ_z. \quad (131)$$

The variance of the phase difference,

$$\text{Var}(\phi) = \frac{1}{n} + k^2 \text{Var}(\Delta N). \quad (132)$$

For an atomic CSS, $\text{Var}(\Delta N) = N_A$. Finally, use n_1 photons to measure J_z to obtain a measurement result of ϕ_1 , then use n_2 photons to measure J_z to obtain a measurement result of ϕ_2 on the same atomic ensemble can create a conditionally spin squeezed atomic state. The projection noise has been reduced to $-(5.3 \pm 0.6)$ dB and metrologically relevant spin squeezing of $-(3.4 \pm 0.7)$ dB on the Cs microwave clock transition has been realized.

In addition to the above measurement-based squeezing, it has been demonstrated that spin squeezed states can be produced unconditionally by cavity feedback.²⁰⁷ The cavity feedback method generates spin dynamics²⁰⁸ similar to the one-axis twisting.¹²² By using the spin squeezed states prepared by cavity feedback method, it has been achieved a high-precision atomic clock of an ensemble of laser-cooled ^{87}Rb atoms beyond the SQL.²⁰⁹ The Allan deviation spectrum indicates that the clock has a precision 2.8(3) times faster than the SQL for averaging times up to 50 s.

6. Summary and discussion

We have given a brief introduction on quantum metrology with cold atoms both in theory and experiment. We start from the general process of physical measurements in quantum mechanics and then discuss how to estimate an unknown parameter, which is the central goal of metrology. The estimation precision is quantified by the uncertainty, which is determined by the input state, the dynamical evolution process and the readout strategy.

The uncertainty of an estimated parameter is limited by the Cramér-Rao bound, which is related to the Fisher information. For a given input state and dynamical evolution, through optimizing over all possible measurements, there exists an ultimate precision limit determined by the quantum Fisher information.

To illustrate the general procedures of quantum metrology, we have introduced two typical quantum interferometry processes: Mach-Zehnder interferometry and Ramsey interferometry. The measurement precision of the interferometers with non-entangled states is limited by the standard quantum limit (SQL). By employing quantum entanglement, the SQL for the measurement precision can be surpassed by inputting multiparticle entangled states, such as, spin squeezed states, NOON states, entangled coherent states and twin Fock states. In realistic systems of cold atoms, the nonlinearity originated from intrinsic or laser induced atom-atom interactions can be used to generate various entangled states and then one can implement some particular precision measurements with the prepared entangled states.

Although there emerge great achievements in quantum metrology with cold atoms, to implement precision measurements with multiparticle entangled states and build practical quantum devices, there are still lots of important things need to be done. For an example, it is worthwhile to analyze the robustness against the environment effects. Therefore, it is vital to explore the effects to the measurement precision in the presence of decoherence,^{81,111,169,210–215} temperature,²¹⁶ and particle losses.^{99,138,217–220}

Besides to the metrology schemes using entanglement as a resource for beating the SQL, there are some alternative entanglement-free schemes beating the SQL. By replacing entangled input states with multiple applications of the phase shift on unentangled single-photon states, the Heisenberg-limited phase estimation has been demonstrated.²²¹ By coupling the quantum resources to a common environment that can be measured at least in part, it has been shown that the Heisenberg-limited measurements can be achieved.²²²

Beyond measuring single parameters in most metrology schemes, it is also possible to estimate simultaneously multiple parameters in some particular metrology schemes. Based upon a discretized phase imaging model, which is an interferometer of $(d + 1)$ modes, d independent phases are possible to be estimated simultaneously.²²³ The theoretical analysis shows that, (i) the quantum strategies for both independent and simultaneous parameter estimation follow the Heisenberg scaling in the total number of

photons for the total variance, and (ii) simultaneous quantum phase estimation improves the precision linearly with the number of phases (i.e. scaling as $\sim 1/d$). Based upon a three-dimensional waveguide, a three-arm interferometer has been proposed to achieve the simultaneous two-parameter estimation.²²⁴ Based upon a two-phase spin rotation, the joint and sequential quantum estimations of the two phases have been studied and the results show the joint estimation method gives a better sensitivity.²²⁵

Lastly, we would like to point out that there are also some metrology schemes realizable with cold atoms alternative to interferometry. By calculating the quantum Fisher information matrix for quantum gases, the sensitivity of measuring the temperature and the chemical potentials of quantum gases has been investigated.²²⁶ The analysis shows that the SQL can be surpassed by using bosonic gases, but not for fermionic gases. The experimental realization of thermometry with Bose condensed atoms has been reported by MIT.²²⁷ Based upon detection of Larmor spin precession of optically pumped atoms in a magnetic field, it is possible to detect weak magnetic field in the radio-frequency range.²²⁸⁻²³⁰ For an atomic magnetometer based upon a spinor BEC with a off-resonant optical field, Steinke et al. analyzes how its sensitivity depends on the dispersive interaction between the spinor BEC and the off-resonant optical field.²³¹ More recently, the detection of a weak alternate-current magnetic field has been demonstrated by applying spin-echo techniques to a spin-2 atomic BEC.²³²

Acknowledgement

We thank Zbigniew Ficek, Roberto Floreanini, Ugo Marzolino, Gheorghe Sorin Paraoanu, Christopher Gerry, and Bruno Julia-Diaz for their useful comments and suggestion. This work is supported by the NBRPC under Grant No. 2012CB821305, the NNSFC under Grants No. 11075223 and No. 11374375, the NCETPC under Grant No. NCET-10-0850, and the Ph.D. Programs Foundation of Ministry of Education of China under Grant No. 20120171110022.

References

1. J. Fortágh and C. Zimmermann, Magnetic microtraps for ultracold atoms, *Rev. Mod. Phys.* **79**, 235 (2007).
2. C. Chin, R. Grimm, P. Julienne, and E. Tiesinga, Feshbach resonances in ultracold gases, *Rev. Mod. Phys.* **82**, 1225 (2010).

3. I. Bloch, J. Dalibard, and W. Zwerger, Many-body physics with ultracold gases, *Rev. Mod. Phys.* **80**, 885 (2008).
4. A. D. Cronin, J. Schmiedmayer, and D. E. Pritchard, Optics and interferometry with atoms and molecules, *Rev. Mod. Phys.* **81**, 1051 (2009).
5. J. P. Dowling and G. J. Milburn, Quantum technology: the second quantum revolution, *Phil. Trans. R. Soc. Lond. A* **361**, 1655 (2003).
6. C. Gross, T. Zibold, E. Nicklas, J. Estève, and M. K. Oberthaler, Nonlinear atom interferometer surpasses classical precision limit, *Nature* **464**, 1165 (2010).
7. M. F. Riedel, P. Bohi, Y. Li, T. W. Hansch, A. Sinatra, and P. Treutlein, Atom-chip-based generation of entanglement for quantum metrology, *Nature* **464**, 1170 (2010).
8. A. Louchet-Chauvet, J. Appel, J. J. Renema, D. Oblak, N. Kjaergaard, and E. S. Polzik, Entanglement-assisted atomic clock beyond the projection noise limit, *New J. Phys.* **12**, 065032 (2010).
9. J. Appel, P. J. Windpassinger, D. Oblak, U. B. Hoff, N. Kjaergaard, and E. S. Polzik, Mesoscopic atomic entanglement for precision measurements beyond the standard quantum limit, *PNAS* **106**, 10960 (2009).
10. B. Lücke, M. Scherer, J. Kruse, L. Pezzé, F. Deuretzbacher, P. Hyllus, O. Topic, J. Peise, W. Ertmer, J. Arlt, L. Santos, A. Smerzi, and C. Klempt, Twin matter waves for interferometry beyond the classical limit, *Science* **334**, 773 (2011).
11. V. Giovannetti, S. Lloyd, and L. Maccone, Quantum-enhanced measurements: Beating the standard quantum limit, *Science* **306**, 1330 (2004).
12. V. Giovannetti, S. Lloyd, and L. Maccone, Quantum metrology, *Phys. Rev. Lett.* **96**, 010401 (2006).
13. V. Giovannetti, S. Lloyd, and L. Maccone, Advances in quantum metrology, *Nat. Photon.* **5**, 222 (2011).
14. D. J. Wineland, J. J. Bollinger, W. M. Itano, F. L. Moore, and D. J. Heinzen, Spin squeezing and reduced quantum noise in spectroscopy, *Phys. Rev. A* **46**, R6797 (1992).
15. A. Sørensen, L.-M. Duan, J. I. Cirac, and P. Zoller, Many-particle entanglement with Bose-Einstein condensates, *Nature* **409**, 63 (2001).
16. C. Lee, Adiabatic Mach-Zehnder interferometry on a quantized Bose-Josephson junction, *Phys. Rev. Lett.* **97**, 150402 (2006).
17. T. Nagata, R. Okamoto, J. L. O'Brien, K. Sasaki, and S. Takeuchi, Beating the standard quantum limit with four-entangled photons, *Science* **316**, 726 (2007).
18. S. Boixo, A. Datta, M. J. Davis, S. T. Flammia, A. Shaji, and C. M. Caves, Quantum metrology: Dynamics versus entanglement, *Phys. Rev. Lett.* **101**, 040403 (2008).
19. L. Pezzé and A. Smerzi, Entanglement, nonlinear dynamics, and the heisenberg limit, *Phys. Rev. Lett.* **102**, 100401 (2009).
20. P. Hyllus, L. Pezzé, and A. Smerzi, Entanglement and sensitivity in precision measurements with states of a fluctuating number of particles, *Phys. Rev. Lett.* **105**, 120501 (2010).

21. G. Y. Xiang, B. L. Higgins, D. W. Berry, H. M. Wiseman, and G. J. Pryde, Entanglement-enhanced measurement of a completely unknown optical phase, *Nat. Photon.* **5**, 43 (2011).
22. M. Napolitano, M. Koschorreck, B. Dubost, N. Behbood, R. J. Sewell, and M. W. Mitchell, Interaction-based quantum metrology showing scaling beyond the Heisenberg limit, *Nature* **471**, 486 (2011).
23. C. Gross, H. Strobel, E. Nicklas, T. Zibold, N. Bar-Gill, G. Kurizki, and M. K. Oberthaler, Atomic homodyne detection of continuous-variable entangled twin-atom states, *Nature* **480**, 219 (2011).
24. Y. M. Hu, M. Feng, and C. Lee, Adiabatic Mach-Zehnder interferometer via an array of trapped ions, *Phys. Rev. A* **85**, 043604 (2012).
25. C. Lee, J. Huang, H. Deng, H. Dai, and J. Xu, Nonlinear quantum interferometry with Bose condensed atoms, *Front. Phys.* **7**, 109 (2012).
26. C. Gross, Spin squeezing, entanglement and quantum metrology with Bose-Einstein condensates, *J. Phys. B: At. Mol. Opt. Phys.* **45**, 103001 (2012).
27. A. J. Leggett, Bose-Einstein condensation in the alkali gases: Some fundamental concepts, *Rev. Mod. Phys.* **73**, 307 (2001).
28. A. Griffin, D. W. Snoke, and S. Stringari, *Bose-Einstein Condensation*, Cambridge University Press (1995).
29. C. J. Pethick and H. Smith, *Bose-Einstein Condensation in Dilute Gases*, Cambridge University Press (2002).
30. C. F. Roos, M. Chwalla, K. Kim, M. Riebe, and R. Blatt, 'Designer atoms' for quantum metrology, *Nature* **443**, 316 (2006).
31. H. Yonezawa, D. Nakane, T. A. Wheatley, K. Iwasawa, S. Takeda, H. Arao, K. Ohki, K. Tsumura, D. W. Berry, T. C. Ralph, H. M. Wiseman, E. H. Huntington, and A. Furusawa, Quantum-enhanced optical-phase tracking, *Science* **337**, 1514 (2012).
32. Y. Torii, Y. Suzuki, M. Kozuma, T. Sugiura, T. Kuga, L. Deng, and E. W. Hagley, Mach-Zehnder bragg interferometer for a Bose-Einstein condensate, *Phys. Rev. A* **61**, 041602 (2000).
33. J. J. Cooper, D. W. Hallwood, and J. A. Dunningham, Entanglement-enhanced atomic gyroscope, *Phys. Rev. A* **81**, 043624 (2010).
34. M. D. Swallows, M. Bishof, Y. Lin, S. Blatt, M. J. Martin, A. M. Rey, and J. Ye, Suppression of collisional shifts in a strongly interacting lattice clock, *Science* **331**, 1043 (2011).
35. M. J. Martin, M. Bishof, M. D. Swallows, X. Zhang, C. Benko, J. von Stecher, A. V. Gorshkov, A. M. Rey, and J. Ye, A quantum many-body spin system in an optical lattice clock, *Science* **341**, 632 (2013).
36. A. André, A. S. Sørensen, and M. D. Lukin, Stability of atomic clocks based on entangled atoms, *Phys. Rev. Lett.* **92**, 230801 (2004).
37. S. Simmons, J. A. Jones, S. D. Karlen, A. Ardavan, and J. J. L. Morton, Magnetic field sensors using 13-spin cat states, *Phys. Rev. A* **82**, 022330 (2010).
38. H. T. Ng, Quantum-limited measurement of magnetic-field gradient with entangled atoms, *Phys. Rev. A* **87**, 043602 (2013).
39. W. Wasilewski, K. Jensen, H. Krauter, J. J. Renema, M. V. Balabas, and

- E. S. Polzik, Quantum noise limited and entanglement-assisted magnetometry, *Phys. Rev. Lett.* **104**, 133601 (2010).
40. C. F. Ockeloen, R. Schmied, M. F. Riedel, and P. Treutlein, Quantum metrology with a scanning probe atom interferometer, arXiv:1303.1313.
 41. H. J. Kimble, Y. Levin, A. B. Matsko, K. S. Thorne, and S. P. Vyatchanin, Conversion of conventional gravitational-wave interferometers into quantum nondemolition interferometers by modifying their input and/or output optics, *Phys. Rev. D* **65**, 022002 (2001).
 42. M.-K. Zhou, Z.-K. Hu, X.-C. Duan, B.-L. Sun, J.-B. Zhao, and J. Luo, Precisely mapping the magnetic field gradient in vacuum with an atom interferometer, *Phys. Rev. A* **82**, 061602 (2010).
 43. M.-K. Zhou, Z.-K. Hu, X.-C. Duan, B.-L. Sun, L.-L. Chen, Q.-Z. Zhang, and J. Luo, Performance of a cold-atom gravimeter with an active vibration isolator, *Phys. Rev. A* **86**, 043630 (2012).
 44. H. Müntinga, H. Ahlers, M. Krutzik, A. Wenzlawski, S. Arnold, D. Becker, K. Bongs, H. Dittus, H. Duncker, N. Gaaloul, C. Gherasim, E. Giese, C. Grzeschik, T. W. Hänsch, O. Hellmig, W. Herr, S. Herrmann, E. Kajari, S. Kleinert, C. Lämmerzahl, W. Lewoczko-Adamczyk, J. Malcolm, N. Meyer, R. Nolte, A. Peters, M. Popp, J. Reichel, A. Roura, J. Rudolph, M. Schiemangk, M. Schneider, S. T. Seidel, K. Sengstock, V. Tamma, T. Valenzuela, A. Vogel, R. Walsler, T. Wendrich, P. Windpassinger, W. Zeller, T. van Zoest, W. Ertmer, W. P. Schleich, and E. M. Rasel, Interferometry with Bose-Einstein condensates in microgravity, *Phys. Rev. Lett.* **110**, 093602 (2013).
 45. A.S.Holevo, *Probabilistic and statistical aspects of quantum theory* vol. 1, *North-Holland Series in Statistics and Probability*, North-Holland, North-Holland Publishing Company, Amsterdam (1982).
 46. C. M. Caves, Quantum-mechanical noise in an interferometer, *Phys. Rev. D* **23**, 1693 (1981).
 47. A. N. Boto, P. Kok, D. S. Abrams, S. L. Braunstein, C. P. Williams, and J. P. Dowling, Quantum interferometric optical lithography: Exploiting entanglement to beat the diffraction limit, *Phys. Rev. Lett.* **85**, 2733 (2000).
 48. H. Lee, P. Kok, and J. P. Dowling, A quantum rosetta stone for interferometry, *J. Mod. Opt.* **49** (2002).
 49. M. Zwiernik, C. A. Pérez-Delgado, and P. Kok, General optimality of the Heisenberg limit for quantum metrology, *Phys. Rev. Lett.* **105**, 180402 (2010).
 50. L. Maccone and V. Giovannetti, Quantum metrology: Beauty and the noisy beast, *Nature Phys.* **7**, 376 (2011).
 51. J. H. Shapiro, S. R. Shepard, and N. C. Wong, Ultimate quantum limits on phase measurement, *Phys. Rev. Lett.* **62**, 2377 (1989).
 52. B. M. Escher, R. L. de Matos Filho, and L. Davidovich, General framework for estimating the ultimate precision limit in noisy quantum-enhanced metrology, *Nature Phys.* **7**, 406 (2011).
 53. Helstrom, *Quantum detection and estimation theory*, Academic Press (1976).

54. B. W. L. Pieter Kok, *Introduction to Optical Quantum Information Processing*, Cambridge University Press (2010).
55. S. L. Braunstein and C. M. Caves, Statistical distance and the geometry of quantum states, *Phys. Rev. Lett.* **72**, 3439 (1994).
56. S. L. Braunstein, C. M. Caves, and G. J. Milburn, Generalized uncertainty relations: theory, examples, and lorentz invariance, *Ann. Phys.* **247**, 135 (1996).
57. S. Boixo, S. T. Flammia, C. M. Caves, and J. Geremia, Generalized limits for single-parameter quantum estimation, *Phys. Rev. Lett.* **98**, 090401 (2007).
58. H. Cramér, *Mathematical Methods of Statistics*, Princeton University Press (1946).
59. S. L. Braunstein, Quantum limits on precision measurements of phase, *Phys. Rev. Lett.* **69**, 3598 (1992).
60. R. A. Fisher, On the mathematical foundations of theoretical statistics, *Phil. Trans. R. Soc. A.* **222**, 309 (1922).
61. R. A. Fisher, Theory of statistical estimation, *Proc. Camb. Phil. Soc.* **22**, 700 (1925).
62. B. M. Escher, R. L. de Matos Filho, and L. Davidovich, Quantum metrology for noisy systems, *Braz. J. Phys.* **41**, 229 (2011).
63. M. A. Nielsen and I. L. Chuang, *Quantum Computation and Quantum Information*, Cambridge University Press (2001).
64. B. M. Escher, L. Davidovich, N. Zagury, and R. L. de Matos Filho, Quantum metrological limits via a variational approach, *Phys. Rev. Lett.* **109**, 190404 (2012).
65. A. Rivas and A. Luis, Precision quantum metrology and nonclassicality in linear and nonlinear detection schemes, *Phys. Rev. Lett.* **105**, 010403 (2010).
66. S. Boixo, A. Datta, M. J. Davis, A. Shaji, A. B. Tacla, and C. M. Caves, Quantum-limited metrology and Bose-Einstein condensates, *Phys. Rev. A* **80**, 032103 (2009).
67. R. Demkowicz-Dobrzański, Optimal phase estimation with arbitrary *a priori* knowledge, *Phys. Rev. A* **83**, 061802 (2011).
68. U. Dorner, R. Demkowicz-Dobrzański, B. J. Smith, J. S. Lundeen, W. Wasilewski, K. Banaszek, and I. A. Walmsley, Optimal quantum phase estimation, *Phys. Rev. Lett.* **102**, 040403 (2009).
69. R. Demkowicz-Dobrzański, U. Dorner, B. J. Smith, J. S. Lundeen, W. Wasilewski, K. Banaszek, and I. A. Walmsley, Quantum phase estimation with lossy interferometers, *Phys. Rev. A* **80**, 013825 (2009).
70. G. S. Paraoanu, Generalized partial measurements, *EPL* **93**, 64002 (2011).
71. J.-W. Pan, Z.-B. Chen, C.-Y. Lu, H. Weinfurter, A. Zeilinger, and M. Żukowski, Multiphoton entanglement and interferometry, *Rev. Mod. Phys.* **84**, 777 (2012).
72. H. F. Hofmann, All path-symmetric pure states achieve their maximal phase sensitivity in conventional two-path interferometry, *Phys. Rev. A* **79**, 033822 (2009).
73. Z. Hradil, R. Myška, J. Peřina, M. Zawisky, Y. Hasegawa, and H. Rauch, Quantum phase in interferometry, *Phys. Rev. Lett.* **76**, 4295 (1996).

74. S. Gasparinetti, P. Solinas, and J. P. Pekola, Geometric Landau-Zener interferometry, *Phys. Rev. Lett.* **107**, 207002 (2011).
75. L. Pezzé, A. Smerzi, G. Khoury, J. F. Hodelin, and D. Bouwmeester, Phase detection at the quantum limit with multiphoton Mach-Zehnder interferometry, *Phys. Rev. Lett.* **99**, 223602 (2007).
76. G. A. Durkin and J. P. Dowling, Local and global distinguishability in quantum interferometry, *Phys. Rev. Lett.* **99**, 070801 (2007).
77. N. F. Ramsey, A molecular beam resonance method with separated oscillating fields, *Phys. Rev.* **78**, 695 (1950).
78. N. F. Ramsey, A new molecular beam resonance method, *Phys. Rev.* **76**, 996 (1949).
79. I. I. Rabi, S. Millman, P. Kusch, and J. R. Zacharias, The molecular beam resonance method for measuring nuclear magnetic moments. the magnetic moments of ${}^3\text{Li}^6$, ${}^3\text{Li}^7$ and ${}^9\text{F}^{19}$, *Phys. Rev.* **55**, 526 (1939).
80. C. J. Foot, *Atomic Physics*, Oxford University Press (2005).
81. G. Ferrini, D. Spehner, A. Minguzzi, and F. W. J. Hekking, Effect of phase noise on quantum correlations in Bose-Josephson junctions, *Phys. Rev. A* **84**, 043628 (2011).
82. M. J. Holland and K. Burnett, Interferometric detection of optical phase shifts at the heisenberg limit, *Phys. Rev. Lett.* **71**, 1355 (1993).
83. D. W. Berry, H. M. Wiseman, and J. K. Breslin, Optimal input states and feedback for interferometric phase estimation, *Phys. Rev. A* **63**, 053804 (2001).
84. L. Pezzé and A. Smerzi, Ultrasensitive two-mode interferometry with single-mode number squeezing, *Phys. Rev. Lett.* **110**, 163604 (2013).
85. D. Leibfried, B. DeMarco, V. Meyer, M. Rowe, A. Ben-Kish, J. Britton, W. M. Itano, B. Jelenković, C. Langer, T. Rosenband, and D. J. Wineland, Trapped-ion quantum simulator: Experimental application to nonlinear interferometers, *Phys. Rev. Lett.* **89**, 247901 (2002).
86. L. Pezzé and A. Smerzi, Phase sensitivity of a Mach-Zehnder interferometer, *Phys. Rev. A* **73**, 011801 (2006).
87. M. B. Serge Haroche and J.-M. Raimond, Atomic clocks for controlling light fields, *Phys. Today* **66**, 27 (2013).
88. D. Kleppner, Norman Ramsey and his method, *Phys. Today* **66**, 25 (2013).
89. N. F. Ramsey, The method of successive oscillatory fields, *Phys. Today* **66**, 36 (2013).
90. J. J. Bollinger, W. M. Itano, D. J. Wineland, and D. J. Heinzen, Optimal frequency measurements with maximally correlated states, *Phys. Rev. A* **54**, R4649 (1996).
91. M. J. Holland and K. Burnett, Interferometric detection of optical phase shifts at the Heisenberg limit, *Phys. Rev. Lett.* **71**, 1355 (1993).
92. L.-M. Kuang and X. Chen, Phase-coherent states and their squeezing properties, *Phys. Rev. A* **50**, 4228 (1994).
93. S. F. Huelga, C. Macchiavello, T. Pellizzari, A. K. Ekert, M. B. Plenio, and J. I. Cirac, Improvement of frequency standards with quantum entanglement, *Phys. Rev. Lett.* **79**, 3865 (1997).

94. C. C. Gerry, Heisenberg-limit interferometry with four-wave mixers operating in a nonlinear regime, *Phys. Rev. A* **61**, 043811 (2000).
95. D. W. Berry and H. M. Wiseman, Optimal states and almost optimal adaptive measurements for quantum interferometry, *Phys. Rev. Lett.* **85**, 5098 (2000).
96. R. A. Campos, C. C. Gerry, and A. Benmoussa, Optical interferometry at the Heisenberg limit with twin fock states and parity measurements, *Phys. Rev. A* **68**, 023810 (2003).
97. X. Wang and B. C. Sanders, Relations between bosonic quadrature squeezing and atomic spin squeezing, *Phys. Rev. A* **68**, 033821 (2003).
98. A. M. Dudarev, R. B. Diener, B. Wu, M. G. Raizen, and Q. Niu, Entanglement generation and multiparticle interferometry with neutral atoms, *Phys. Rev. Lett.* **91**, 010402 (2003).
99. S. D. Huver, C. F. Wildfeuer, and J. P. Dowling, Entangled Fock states for robust quantum optical metrology, imaging, and sensing, *Phys. Rev. A* **78**, 063828 (2008).
100. D. Meiser and M. J. Holland, Robustness of Heisenberg-limited interferometry with balanced fock states, *New J. Phys.* **11**, 033002 (2009).
101. H. Cable and G. A. Durkin, Parameter estimation with entangled photons produced by parametric down-conversion, *Phys. Rev. Lett.* **105**, 013603 (2010).
102. C. C. Gerry and J. Mimih, Heisenberg-limited interferometry with pair coherent states and parity measurements, *Phys. Rev. A* **82**, 013831 (2010).
103. P. M. Anisimov, G. M. Raterman, A. Chiruvelli, W. N. Plick, S. D. Huver, H. Lee, and J. P. Dowling, Quantum metrology with two-mode squeezed vacuum: Parity detection beats the Heisenberg limit, *Phys. Rev. Lett.* **104**, 103602 (2010).
104. K. P. Seshadreesan, P. M. Anisimov, H. Lee, and J. P. Dowling, Parity detection achieves the Heisenberg limit in interferometry with coherent mixed with squeezed vacuum light, *New J. Phys.* **13** (2011).
105. Y. Ben-Aryeh, Phase estimation by photon counting measurements in the output of a linear Mach-Zehnder interferometer, *J. Opt. Soc. Am. B.* **29**, 2754 (2012).
106. J. Kong, Z. Y. Ou, and W. Zhang, Phase-measurement sensitivity beyond the standard quantum limit in an interferometer consisting of a parametric amplifier and a beam splitter, *Phys. Rev. A* **87**, 023825 (2013).
107. F. T. Arecchi, E. Courtens, R. Gilmore, and H. Thomas, Atomic coherent states in quantum optics, *Phys. Rev. A* **6**, 2211 (1972).
108. J. J. Sakurai, *Modern Quantum Mechanics*, New York: Addison-Wesley (1993).
109. J. M. Radcliffe, Some properties of coherent spin states, *J. Phys. A.* **4**, 313 (1971).
110. W.-M. Zhang, D. H. Feng, and R. Gilmore, Coherent states: Theory and some applications, *Rev. Mod. Phys.* **62**, 867 (1990).
111. Y. C. Liu, G. R. Jin, and L. You, Quantum-limited metrology in the presence of collisional dephasing, *Phys. Rev. A* **82**, 045601 (2010).

112. D. J. Wineland, J. J. Bollinger, W. M. Itano, and D. J. Heinzen, Squeezed atomic states and projection noise in spectroscopy, *Phys. Rev. A* **50**, 67 (1994).
113. T. Kim, O. Pfister, M. J. Holland, J. Noh, and J. L. Hall, Influence of decorrelation on Heisenberg-limited interferometry with quantum correlated photons, *Phys. Rev. A* **57**, 4004 (1998).
114. D. F. Walls, Squeezed states of light, *Nature* **306**, 141 (1983).
115. C. A. Sackett, Quantum measurement: A condensate's main squeeze, *Nature* **464**, 1133 (2010).
116. M. Hillery and M. S. Zubairy, Entanglement conditions for two-mode states, *Phys. Rev. Lett.* **96**, 050503 (2006).
117. X. Wang and B. C. Sanders, Spin squeezing and pairwise entanglement for symmetric multiqubit states, *Phys. Rev. A* **68**, 012101 (2003).
118. G.-R. Jin and S. W. Kim, Storage of spin squeezing in a two-component Bose-Einstein condensate, *Phys. Rev. Lett.* **99**, 170405 (2007).
119. A. S. Sørensen and K. Mølmer, Entanglement and extreme spin squeezing, *Phys. Rev. Lett.* **86**, 4431 (2001).
120. J. Ma, X. Wang, C. Sun, and F. Nori, Quantum spin squeezing, *Physics Reports* **509**, 89 (2011).
121. D. F. Walls and P. Zoller, Reduced quantum fluctuations in resonance fluorescence, *Phys. Rev. Lett.* **47**, 709 (1981).
122. M. Kitagawa and M. Ueda, Squeezed spin states, *Phys. Rev. A* **47**, 5138 (1993).
123. X. Wang, A. S. Sørensen, and K. Mølmer, Spin squeezing in the Ising model, *Phys. Rev. A* **64**, 053815 (2001).
124. A. Messikh, Z. Ficek, and M. R. B. Wahiddin, Spin squeezing as a measure of entanglement in a two-qubit system, *Phys. Rev. A* **68**, 064301 (2003).
125. D. Ulam-Orgikh and M. Kitagawa, Spin squeezing and decoherence limit in Ramsey spectroscopy, *Phys. Rev. A* **64**, 052106 (2001).
126. K. Banaszek, R. Demkowicz-Dobrzanski, and I. A. Walmsley, Quantum states made to measure, *Nat. Photon.* **3**, 673 (2009).
127. Z. Ji, G. Wang, R. Duan, Y. Feng, and M. Ying, Parameter estimation of quantum channels, *IEEE TRANSACTIONS ON INFORMATION THEORY* **54**, 5172 (2008).
128. A. Shaji and C. M. Caves, Qubit metrology and decoherence, *Phys. Rev. A* **76**, 032111 (2007).
129. G. Meng, H. Xu, S. Yang, S. Zhang, G. Guo, B. Shi, and X. Zou, Fast generation of many-atom maximal entanglement in spin-1 Bose-Einstein condensates, *Phys. Rev. A* **85**, 035601 (2012).
130. I. Afek, O. Ambar, and Y. Silberberg, High-NOON states by mixing quantum and classical light, *Science* **328**, 879 (2010).
131. B. C. Sanders, Review of entangled coherent states, *J. Phys. A* **45**, 244002 (2012).
132. B. C. Sanders, Entangled coherent states, *Phys. Rev. A* **45**, 6811 (1992).
133. J. Joo, W. J. Munro, and T. P. Spiller, Quantum metrology with entangled coherent states, *Phys. Rev. Lett.* **107**, 083601 (2011).

134. J. A. Dunningham, K. Burnett, and S. M. Barnett, Interferometry below the standard quantum limit with Bose-Einstein condensates, *Phys. Rev. Lett.* **89**, 150401 (2002).
135. J. A. Dunningham and K. Burnett, Sub-shot-noise-limited measurements with Bose-Einstein condensates, *Phys. Rev. A* **70**, 033601 (2004).
136. C. C. Gerry and J. Mimih, The parity operator in quantum optical metrology, *Contemporary Physics* **51**, 497 (2010).
137. C. C. Gerry and R. A. Campos, Generation of maximally entangled states of a Bose-Einstein condensate and Heisenberg-limited phase resolution, *Phys. Rev. A* **68**, 025602 (2003).
138. Y. Li, P. Treutlein, J. Reichel, and A. Sinatra, Spin squeezing in a bimodal condensate: spatial dynamics and particle losses, *Eur. Phys. J. B* **68**, 365 (2009).
139. R. Bucker, J. Grond, S. Manz, T. Berrada, T. Betz, C. Koller, U. Hohenester, T. Schumm, A. Perrin, and J. Schmiedmayer, Twin-atom beams, *Nature Phys.* **7**, 608 (2011).
140. J. J. Cooper, D. W. Hallwood, J. A. Dunningham, and J. Brand, Robust quantum enhanced phase estimation in a multimode interferometer, *Phys. Rev. Lett.* **108**, 130402 (2012).
141. M. Rab, A. L. C. Hayward, J. H. Cole, A. D. Greentree, and A. M. Martin, Interferometry using adiabatic passage in dilute-gas Bose-Einstein condensates, *Phys. Rev. A* **86**, 063605 (2012).
142. J. Grond, U. Hohenester, J. Schmiedmayer, and A. Smerzi, Mach-Zehnder interferometry with interacting trapped Bose-Einstein condensates, *Phys. Rev. A* **84**, 023619 (2011).
143. V. Meyer, M. A. Rowe, D. Kielpinski, C. A. Sackett, W. M. Itano, C. Monroe, and D. J. Wineland, Experimental demonstration of entanglement-enhanced rotation angle estimation using trapped ions, *Phys. Rev. Lett.* **86**, 5870 (2001).
144. D. Leibfried, M. D. Barrett, T. Schaetz, J. Britton, J. Chiaverini, W. M. Itano, J. D. Jost, C. Langer, and D. J. Wineland, Toward Heisenberg-limited spectroscopy with multiparticle entangled states, *Science* **304**, 1476 (2004).
145. I. M. Julian Grond, Ulrich Hohenester and J. Schmiedmayer, Atom interferometry with trapped Bose-Einstein condensates: impact of atom-atom interactions, *New J. Phys.* **12**, 065036 (2010).
146. C. Orzel, A. K. Tuchman, M. L. Fenselau, M. Yasuda, and M. A. Kasevich, Squeezed states in a Bose-Einstein condensate, *Science* **291**, 2386 (2001).
147. J. Estève, C. Gross, A. Weller, S. Giovanazzi, and M. K. Oberthaler, Squeezing and entanglement in a Bose-Einstein condensate, *Nature* **455**, 1216 (2008).
148. C. Bodet, J. Estève, M. K. Oberthaler, and T. Gasenzer, Two-mode Bose gas: Beyond classical squeezing, *Phys. Rev. A* **81**, 063605 (2010).
149. B. Zeng, D. L. Zhou, Z. Xu, and L. You, Entanglement and spin-squeezing properties for three bosons in two modes, *Phys. Rev. A* **71**, 042317 (2005).
150. O. E. Müstecaplıoğlu, M. Zhang, and L. You, Spin squeezing and entanglement in spinor condensates, *Phys. Rev. A* **66**, 033611 (2002).

151. L. You, Creating maximally entangled atomic states in a Bose-Einstein condensate, *Phys. Rev. Lett.* **90**, 030402 (2003).
152. Y.-C. Liu, G.-R. Jin, and W.-M. Liu, Spin squeezing in a generalized one-axis twisting model, *New J. Phys.* **11**, 073049 (2009).
153. Y. C. Liu, Z. F. Xu, G. R. Jin, and L. You, Spin squeezing: Transforming one-axis twisting into two-axis twisting, *Phys. Rev. Lett.* **107**, 013601 (2011).
154. F. Benatti, R. Floreanini, and U. Marzolino, Sub-shot-noise quantum metrology with entangled identical particles Original, *Ann. Phys.*, **325**, 924 (2010).
155. F. Benatti, R. Floreanini, and U. Marzolino, Entanglement and squeezing with identical particles: ultracold atom quantum metrology, *J. Phys. B* **44**, 091001 (2011).
156. G. Argentieri, F. Benatti, R. Floreanini, and U. Marzolino, Entangled identical particles and noise, *Int. J. Quantum Inform.* **09**, 1745 (2011).
157. Y. Khodorkovsky, G. Kurizki, and A. Vardi, Decoherence and entanglement in a bosonic Josephson junction Bose-enhanced quantum Zeno control of phase diffusion, *Phys. Rev. A* **80**, 023609 (2009).
158. A. Smerzi, S. Fantoni, S. Giovanazzi, and S. R. Shenoy, Quantum coherent atomic tunneling between two trapped Bose-Einstein condensates, *Phys. Rev. Lett.* **79**, 4950 (1997).
159. G. J. Milburn, J. Corney, E. M. Wright, and D. F. Walls, Quantum dynamics of an atomic Bose-Einstein condensate in a double-well potential, *Phys. Rev. A* **55**, 4318 (1997).
160. M. J. Steel and M. J. Collett, Quantum state of two trapped Bose-Einstein condensates with a Josephson coupling, *Phys. Rev. A* **57**, 2920 (1998).
161. R. W. Spekkens and J. E. Sipe, Spatial fragmentation of a Bose-Einstein condensate in a double-well potential, *Phys. Rev. A* **59**, 3868 (1999).
162. C. Lee, W. Hai, L. Shi, X. Zhu, and K. Gao, Chaotic and frequency-locked atomic population oscillations between two coupled Bose-Einstein condensates, *Phys. Rev. A* **64**, 053604 (2001).
163. G. S. Paraoanu, S. Kohler, F. Sols, and A. J. Leggett, The Josephson plasmon as a Bogoliubov quasiparticle, *J. Phys. B* **34**, 4689 (2001).
164. C. Lee, W. Hai, L. Shi, and K. Gao, Phase-dependent spontaneous spin polarization and bifurcation delay in coupled two-component Bose-Einstein condensates, *Phys. Rev. A* **69**, 033611 (2004).
165. R. Gati and M. K. Oberthaler, A bosonic Josephson junction, *J. Phys. B* **40**, R61 (2007).
166. C. Lee, L.-B. Fu, and Y. S. Kivshar, Many-body quantum coherence and interaction blockade in Josephson-linked Bose-Einstein condensates, *EPL* **81**, 60006 (2008).
167. L.-B. Fu, D.-F. Ye, C. Lee, W. Zhang, and J. Liu, Adiabatic Rosen-Zener interferometry with ultracold atoms, *Phys. Rev. A* **80**, 013619 (2009).
168. B. Julia-Diaz, D. Dagnino, M. Lewenstein, J. Martorell, and A. Polls, Macroscopic self trapping in BECs: analysis of a dynamical quantum phase transition, *Phys. Rev. A* **81**, 023615 (2010).

169. N. Bar-Gill, G. Kurizki, M. Oberthaler, and N. Davidson, Dynamic control and probing of many-body decoherence in double-well Bose-Einstein condensates, *Phys. Rev. A* **80**, 053613 (2009).
170. C. Lee, Universality and anomalous mean-field breakdown of symmetry-breaking transitions in a coupled two-component condensate, *Phys. Rev. Lett.* **102**, 070401 (2009).
171. Q. Y. He, M. D. Reid, T. G. Vaughan, C. Gross, M. Oberthaler, and P. D. Drummond, Einstein-Podolsky-Rosen entanglement strategies in two-well Bose-Einstein condensates, *Phys. Rev. Lett.* **106**, 120405 (2011).
172. H. T. Ng and S.-I. Chu, Steady-state entanglement in a double-well Bose-Einstein condensate through coupling to a superconducting resonator, *Phys. Rev. A* **84**, 023629 (2011).
173. B. Dalton and S. Ghanbari, Two-mode theory of Bose-Einstein condensates: interferometry and the Josephson model, *J. Mod. Opt.* **59**, 287 (2012).
174. G. R. Jin, Y. An, T. Yan, and Z. S. Lu, Dynamical generation of phase-squeezed states in two-component Bose-Einstein condensates, *Phys. Rev. A* **82**, 063622 (2010).
175. Q. Y. He, S.-G. Peng, P. D. Drummond, and M. D. Reid, Planar quantum squeezing and atom interferometry, *Phys. Rev. A* **84**, 022107 (2011).
176. B. Julia-Diaz, T. Zibold, M. K. Oberthaler, M. Mele-Messeguer, J. Martorell, and A. Polls, Dynamic generation of spin-squeezed states in bosonic Josephson junctions, *Phys. Rev. A* **86**, 023615 (2012).
177. B. Julia-Diaz, E. Torrontegui, J. Martorell, J. G. Muga, and A. Polls, Fast generation of spin-squeezed states in bosonic Josephson junctions, *Phys. Rev. A* **86**, 063623 (2012).
178. I. Tikhonenkov, M. G. Moore, and A. Vardi, Optimal Gaussian squeezed states for atom interferometry in the presence of phase diffusion, *Phys. Rev. A* **82**, 043624 (2010).
179. Y. Li, Y. Castin, and A. Sinatra, Optimum spin squeezing in Bose-Einstein condensates with particle losses, *Phys. Rev. Lett.* **100**, 210401 (2008).
180. A. Sinatra, E. Witkowska, J.-C. Dornstetter, Y. Li, and Y. Castin, Limit of spin squeezing in finite-temperature Bose-Einstein condensates, *Phys. Rev. Lett.* **107**, 060404 (2011).
181. R. Gati, B. Hemmerling, J. Fölling, M. Albiez, and M. K. Oberthaler, Noise thermometry with two weakly coupled Bose-Einstein condensates, *Phys. Rev. Lett.* **96**, 130404 (2006).
182. G. B. Jo, J. H. Choi, C. Christensen, Y. R. Lee, T. Pasquini, W. Ketterle, and D. Pritchard, Matter-wave interferometry with phase fluctuating Bose-Einstein condensates, *Phys. Rev. Lett.* **99**, 240406 (2007).
183. S. Hofferberth, I. Lesanovsky, B. Fischer, J. Verdu, and J. Schmiedmayer, Radiofrequency-dressed-state potentials for neutral atoms, *Nature Phys.* **2**, 710 (2006).
184. S. Hofferberth, I. Lesanovsky, T. Schumm, A. Imambekov, V. Gritsev, E. Demler, and J. Schmiedmayer, Probing quantum and thermal noise in an interacting many-body system, *Nature Phys.* **4**, 489 (2008).
185. G. B. Jo, Y. Shin, S. Will, T. Pasquini, M. Saba, W. Ketterle, D. Pritchard,

- M. Vengalattore, and M. Prentiss, Long phase coherence time and number squeezing of two Bose-Einstein condensates on an atom chip, *Phys. Rev. Lett.* **98**, 030407 (2007).
186. J. Estève, C. Gross, A. Weller, S. Giovanazzi, and M. K. Oberthaler, Squeezing and entanglement in a Bose-Einstein condensate, *Nature* **455**, 1216 (2008).
187. Z. Hadzibabic, S. Stock, B. Battelier, V. Bretin, and J. Dalibard, Interference of an array of independent Bose-Einstein condensates, *Phys. Rev. Lett.* **93**, 180403 (2004).
188. C. Orzel, A. K. Tuchman, M. L. Fenselau, M. Yasuda, and M. A. Kasevich, Squeezed states in a Bose-Einstein condensate, *Science* **291**, 2386 (2001).
189. Ö. E. Müstecaplıoğlu, W. Zhang, and L. You, Quantum dynamics of a spin-1 condensate in a double-well potential, *Phys. Rev. A* **75**, 023605 (2007).
190. D. J. Wineland, Nobel Lecture: Superposition, entanglement, and raising Schrödinger's cat, *Rev. Mod. Phys.* **85**, 1103 (2013).
191. J. I. Cirac and P. Zoller, Quantum computations with cold trapped ions, *Phys. Rev. Lett.* **74**, 4091 (1995).
192. J. Steinbach and C. C. Gerry, Efficient scheme for the deterministic maximal entanglement of N trapped ions, *Phys. Rev. Lett.* **81**, 5528 (1998).
193. A. Bermudez, P. O. Schmidt, M. B. Plenio, and A. Retzker, Robust trapped-ion quantum logic gates by continuous dynamical decoupling, *Phys. Rev. A* **85**, 040302 (2012).
194. A. Stute, B. Casabone, P. Schindler, T. Monz, P. O. Schmidt, B. Brandstätter, T. E. Northup, and R. Blatt, Tunable ion-photon entanglement in an optical cavity, *Nature* **485**, 482 (2012).
195. B. B. Blinov, D. L. Moehring, L.-M. Duan, and C. Monroe, Observation of entanglement between a single trapped atom and a single photon, *Nature* **428**, 153 (2004).
196. J. Volz, M. Weber, D. Schlenk, W. Rosenfeld, J. Vrana, K. Saucke, C. Kurtsiefer, and H. Weinfurter, Observation of entanglement of a single photon with a trapped atom, *Phys. Rev. Lett.* **96**, 030404 (2006).
197. R. Blatt and D. J. Wineland, Entangled States of Trapped Atomic Ions, *Nature* **453**, 1008 (2008).
198. R. Blatt and C. F. Roos, Quantum simulations with trapped ions, *Nature Phys.* **8**, 277 (2012).
199. Ch. Schneider, D. Porras and T. Schaetz, Experimental quantum simulations of many-body physics with trapped ions, *Rep. Prog. Phys.* **75**, 024401 (2012).
200. H. Häffner, S. Gulde, M. Riebe, G. Lancaster, C. Becher, J. Eschner, F. Schmidt-Kaler, and R. Blatt, Precision measurement and compensation of optical Stark shifts for an ion-trap quantum processor, *Phys. Rev. Lett.* **90**, 143602 (2003).
201. D. J. Wineland and D. Leibfried, Quantum information processing and metrology with trapped ions, *Laser Phys. Lett.* **8**, 175 (2011).
202. Z. Chen, J. G. Bohnet, S. R. Sankar, J. Dai, and J. K. Thompson, Conditional spin squeezing of a large ensemble via the vacuum Rabi splitting,

- Phys. Rev. Lett.* **106**, 133601 (2011).
203. H. Krauter, C. A. Muschik, K. Jensen, W. Wasilewski, J. M. Petersen, J. I. Cirac, and E. S. Polzik, Entanglement generated by dissipation and steady state entanglement of two macroscopic objects, *Phys. Rev. Lett.* **107**, 080503 (2011).
 204. A. Kuzmich, L. Mandel, and N. P. Bigelow, Generation of spin squeezing via continuous quantum nondemolition measurement, *Phys. Rev. Lett.* **85**, 1594 (2000).
 205. J. Hald, J. L. Sørensen, C. Schori, and E. S. Polzik, Spin squeezed atoms: A macroscopic entangled ensemble created by light, *Phys. Rev. Lett.* **83**, 1319 (1999).
 206. C. M. Trail, P. S. Jessen, and I. H. Deutsch, Strongly enhanced spin squeezing via quantum control, *Phys. Rev. Lett.* **105**, 193602 (2010).
 207. I. D. Leroux, M. H. Schleier-Smith, and V. Vuletic, Implementation of cavity squeezing of a collective atomic spin, *Phys. Rev. Lett.* **104**, 073602 (2010).
 208. M. H. Schleier-Smith, I. D. Leroux, and V. Vuletic, Squeezing the collective spin of a dilute atomic ensemble by cavity feedback, *Phys. Rev. A* **81**, 021804(R) (2010).
 209. I. D. Leroux, M. H. Schleier-Smith, and V. Vuletic, Orientation-dependent entanglement lifetime in a squeezed atomic clock, *Phys. Rev. Lett.* **104**, 250801 (2010).
 210. M. G. Genoni, S. Olivares, and M. G. A. Paris, Optical Phase Estimation in the Presence of Phase Diffusion, *Phys. Rev. Lett.* **106**, 153603 (2011).
 211. J. Borregaard and S. Sørensen, Near-Heisenberg-limited atomic clocks in the presence of decoherence, *Phys. Rev. Lett.* **111**, 090801 (2013).
 212. L. Ostermann, H. Ritsch, and C. Genes, Protected state enhanced quantum metrology with interacting two-level ensembles, arXiv:1307.2558.
 213. R. Chaves, J. B. Brask, M. Markiewicz, J. Kolodynski, and A. Actin, Noisy metrology beyond the standard quantum limit, arXiv:1212.3286.
 214. J. Kolodynski and R. Demkowicz-Dobrzanski, Efficient tools for quantum metrology with uncorrelated noise, *New J. Phys.* **15**, 073043 (2013).
 215. S. I. Knysh and G. A. Durkin, Estimation of phase and diffusion: combining quantum statistics and classical noise, arXiv:1307.0470.
 216. A. Sinatra, E. Witkowska, and Y. Castin, Spin squeezing in finite temperature Bose-Einstein condensates: Scaling with the system size, *The European Physical Journal Special Topics*. **203**, 87 (2012).
 217. X.-X. Zhang, Y.-X. Yang, and X.-B. Wang, Lossy quantum-optical metrology with squeezed states, *Phys. Rev. A* **88**, 013838 (2013).
 218. A. Datta, L. Zhang, N. Thomas-Peter, U. Dorner, B. J. Smith, and I. A. Walmsley, Quantum metrology with imperfect states and detectors, *Phys. Rev. A* **83**, 063836 (2011).
 219. L. Maccone and G. De Cillis, Robust strategies for lossy quantum interferometry, *Phys. Rev. A* **79**, 023812 (2009).
 220. N. Spagnolo, C. Vitelli, V. G. Lucivero, V. Giovannetti, L. Maccone, and F. Sciarrino, Phase estimation via quantum interferometry for noisy detectors, *Phys. Rev. Lett.* **108**, 233602 (2012).

221. B. L. Higgins, D. W. Berry, S. D. Bartlett, H. M. Wiseman, and G. J. Pryde, Entanglement-free Heisenberg-limited phase estimation, *Nature* **450**, 393 (2007).
222. D. Braun and J. Martin, Heisenberg-limited sensitivity with decoherence-enhanced measurements, *Nature Commun.* **2**, 223 (2011).
223. P. C. Humphreys, M. Barbieri, A. Datta, and I. A. Walmsley, Quantum enhanced multiple phase estimation, *Phys. Rev. Lett.* **111**, 070403 (2013).
224. N. Spagnolo, L. Aparo, C. Vitelli, A. Crespi, R. Ramponi, R. Osellame, P. Mataloni, and F. Sciarrino, Quantum interferometry with three-dimensional geometry, *Scientific Reports* **2**, 862 (2012).
225. C. Vaneph, T. Tufarelli, and M. G. Genoni, Quantum estimation of a two-phase spin rotation, *Quantum Measurements and Quantum Metrology* **1**, 12 (2013).
226. U. Marzolino and D. Braun, Precision measurements with quantum gases, arXiv:1308.2735.
227. A. E. Leanhardt, T. A. Pasquini, M. Saba, A. Schirotzek, Y. Shin, D. Kielpinski, D. E. Pritchard, and W. Ketterle, Cooling Bose-Einstein condensates below 500 Picokelvin, *Science* **301**, 1513 (2003).
228. I. K. Kominis, T. W. Kornack, J. C. Allred, and M. V. Romalis, A subfemtotesla multichannel atomic magnetometer, *Nature* **422**, 596 (2003).
229. I. M. Savukov, S. J. Seltzer, M. V. Romalis, and K. L. Sauer, Tunable atomic magnetometer for detection of radio-frequency magnetic fields, *Phys. Rev. Lett.* **95**, 063004 (2005).
230. O. Alem, K. L. Sauer, and M. V. Romalis, Spin damping in an RF atomic magnetometer, *Phys. Rev. A* **87**, 013413 (2013).
231. S. K. Steinke, S. Singh, P. Meystre, K. C. Schwab, and M. Vengalattore, Quantum back-action in spinor condensate magnetometry, arXiv:1211.2870.
232. Y. Eto, H. Ikeda, H. Suzuki, S. Hasegawa, Y. Tomiyama, S. Sekine, M. Sadgrove, and T. Hirano, Spin-echo-based magnetometry with spinor Bose-Einstein condensates, arXiv:1306.1011.